

TOPPO: Rethinking PPO for Multi-Task Reinforcement Learning with Critic Balancing

Yuanpeng Li
UC Irvine

Gefei Lin
George Washington University

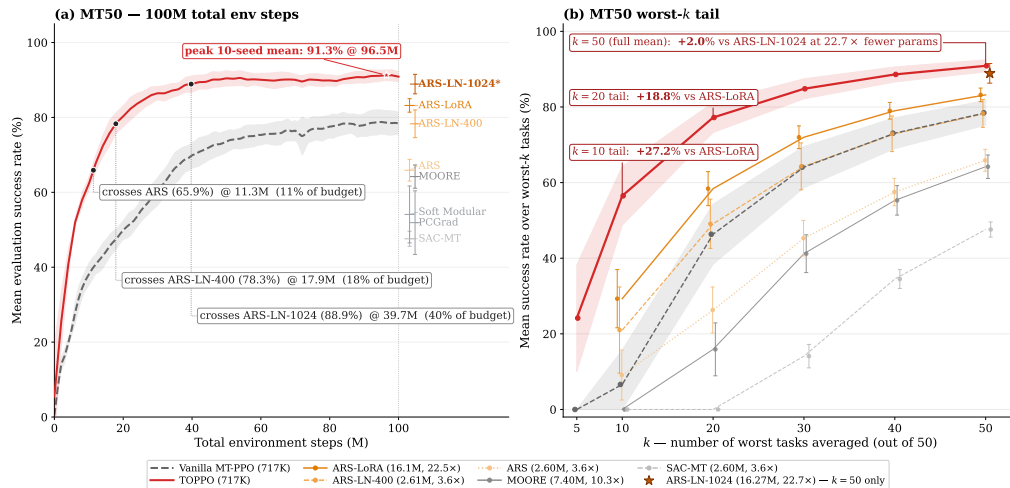
Annie Qu
UC Santa Barbara

Rui Miao[†]
UT Dallas

Code Repository: To be released.

Abstract

Soft Actor-Critic (SAC) and its variants dominate Multi-Task Reinforcement Learning (MTRL) due to their off-policy sample efficiency, while on-policy methods such as Proximal Policy Optimization (PPO) remain underexplored. We diagnose that PPO in MTRL suffers from a previously overlooked issue: critic-side gradient ill-conditioning, which may cause tail tasks to stall while easy tasks dominate the value function’s updates. To address this, we propose TOPPO (Tail-Optimized PPO), a reformulation of PPO via Critic Balancing—a set of modules that improve gradient conditioning and balance learning dynamics across tasks. Unlike prior approaches that rely on modular architectures or large models, TOPPO targets the optimization bottleneck within PPO itself. Empirically, TOPPO achieves stronger mean and tail-task performance than published SAC-family and ARS-family baselines while using substantially fewer parameters and environment steps on Meta-World+ benchmark. Notably, TOPPO matches or surpasses strong SAC baselines early in training and maintains superior performance at full budget. Ablations confirm the effectiveness of each module in TOPPO and provide insights into their interactions. Our results demonstrate that, with proper optimization, on-policy methods can rival or exceed off-policy approaches in MTRL, challenging the prevailing reliance on SAC and highlighting critic-side gradient conditioning as the central bottleneck.



Meta-World+ MT50, V2 rewards; 100M total environment steps. Ours ($n = 10$ seeds); [400, 400, 400] shared MLPs, 717K total parameters. ARS family ($n = 8$ seeds); final-checkpoint numbers reproduced from Cho et al. (ICML 2025), Tables 1 & 2. Worst-k (b): mean over each seed’s k worst tasks, then averaged across seeds.

Figure 1: TOPPO (717K params) on Meta-World V2 MT50 matches the ARS family at 3.6–22.7× fewer parameters. (a) Training curve. (b) Worst- k tail tasks; $k=50$ is the standard MT50 mean.

[†]Corresponding to Rui Miao <rui.miao@utdallas.edu>

1 Introduction

Soft Actor-Critic (SAC) [Haarnoja et al., 2018] has been the default backbone for Multi-Task Reinforcement Learning (MTRL), due to its off-policy nature and sample efficiency under online data-collection budgets: the replay buffer reuses past experiences, and the slow target network softens per-task TD-error magnitudes across history so that cross-task gradient imbalance is not directly visible to the optimizer. On Meta-World [Yu et al., 2020b], the canonical multi-task manipulation benchmark, this preference is near-universal: architectural variants (Soft Modularization [Yang et al., 2020], CARE [Sodhani et al., 2021], PaCo [Sun et al., 2022], MOORE [Hendawy et al., 2024], ARS [Cho et al., 2025]) and gradient-aggregation methods (PCGrad [Yu et al., 2020a], CAGrad [Liu et al., 2021], FAMO [Liu et al., 2023], FairGrad [Ban and Ji, 2024], Nash-MTL [Navon et al., 2022], loss-level reweighting [Kendall et al., 2018, Liu et al., 2019]) all build on SAC-style training [McLean et al., 2025]. Despite this, every published non-ARS multi-task SAC method floors at 0% success rate on the ten hardest MT50 tasks, while the strongest ARS variant clears the floor only at 29.3% and at a substantially higher parameter cost.

In contrast, on-policy methods such as Proximal Policy Optimization (PPO) [Schulman et al., 2017] remain underexplored in MTRL. The original Meta-World Multi-Task PPO (MT-PPO) baseline scored only $\sim 30\%$ on MT10 with a (512, 512) MLP, and this comparison has not been revisited under architectures matched to modern MTRL methods. PPO is also a useful testbed for cross-task gradient ill-conditioning: its on-policy GAE exposes task imbalance at each minibatch, without replay-buffer smoothing or target-network lag. We therefore revisit MT-PPO with a $[400 \times 3]$ backbone, matching CAGrad/CARE/PaCo/MOORE, and find that even vanilla MT-PPO lifts the worst-10 tail above the zero floor of prior non-ARS methods while using far fewer parameters.

Although vanilla MT-PPO already breaks the floor, the hardest tasks remain far from solved, and we trace the remaining gap to a self-reinforcing trap on the critic. Early in training, a few easier tasks learn fast and produce large critic gradients, pulling the shared critic network toward features that reduce their TD errors. Harder tasks that contribute little to this aggregate update must then fit their value functions through shared features optimized primarily for other tasks, which biases their advantage estimates rather than simply making them vanish. The actor updates on those tasks then follow this distorted signal; in the online loop, the resulting policies collect worse or less informative rollouts, leaving the next critic update with little useful signal from the same tasks. Crucially, loss-level or actor-side reweighting methods such as DWA [Liu et al., 2019] and UW [Kendall et al., 2018] cannot break this loop when they leave the critic-gradient geometry uncorrected.

Empirically, per-task critic gradient norms span $\sim 497\times$ across tasks, while per-task actor gradient norms span only $\sim 4.1\times$ after per-task advantage normalization (Figure 2). This asymmetry is stable across training, and concurrent benchmarking work also identifies the critic, not the actor,

Table 1: MT-PPO diagnosis, TOPPO module and mechanism. The main failure is critic-side ill-conditioning D1–D3. The actor row is a residual combiner choice after per-task advantage normalization removes most actor-side scale spread.

Diagnosis	Module / stage	Mechanism and evidence
<i>Critic-side (primary failure)</i>		
D1: Scale Spread	PopArt value-target layer; [van Hasselt et al., 2016, Hessel et al., 2019]	Compresses critic-Gram diagonal scale. Evidence: Figures 3 and D.1, Corollary 1, Table D.1, and Section D.5.
D2: Co-Linear Collapse	LayerNorm-Critic (LN-c) critic representation layer [Ba et al., 2016]; RL precedent [Lee et al., 2025, Hansen et al., 2024]	Regularizes the critic feature Jacobian and lowers critic-Gram off-diagonal cosine collapse while leaving scale structure intact. Evidence: Figures 3, D.1 and D.3.
D3: Unfair Aggregation	FairGrad-Critic (FG-c) $\alpha=1$ critic gradient combiner $\mathbf{G}^c \mathbf{w} = \mathbf{w}^{-1}$ [Ban and Ji, 2024, Mo and Walrand, 2000, Kelly, 1997]	Pins the combined-gradient norm at \sqrt{K} -level and absorbs positive task-wise rescaling at the aggregator output. Evidence: Theorem 1 and Figures D.4 and D.5.
<i>Actor-side (secondary failure)</i>		
Direction Conflict	PCGrad-Actor (PCGrad-a) actor gradient combiner on \mathbf{g}_i^a [Yu et al., 2020a]	Actor norm spread is small, so the actor-side combiner targets negative-cosine pairs rather than scale. Evidence: Figures 2 and D.2 and Table D.2.

as where cross-task gradient conflict concentrates in MT-PPO [Joshi et al., 2025]. The critic ill-conditioning then decomposes into three aspects (Table 1): (D1) per-task gradient-norm spread, (D2) representation-level co-linear collapse in the per-task Gram matrix, and (D3) unfair aggregation of an already-imbalanced gradient set.

To address these three aspects of critic ill-conditioning together with the residual actor-side gradient conflict, we propose TOPPO (Tail-Optimized PPO), which incorporates four modules at four distinct stages of the per-minibatch update (Table 1). PopArt normalizes per-task value targets via a per-task affine head, putting each task’s squared TD loss on a comparable scale before the critic gradients are formed. LN-c adds LayerNorm in the critic to improve hidden-feature conditioning. FairGrad ($\alpha=1$) reweights per-task critic gradients with an α -fair objective, selecting a scale-invariant aggregate critic update. Finally, PCGrad-a handles the remaining actor-side conflict by projecting negative-cosine actor-gradient pairs after advantage normalization.

In our experiments, with only 717K parameters, TOPPO reaches $90.88 \pm 1.59\%$ final-checkpoint mean success on MT50, outperforming ARS-LN-1024 by 1.98% with $22.7\times$ fewer parameters (Table 2). It also reaches $56.50 \pm 7.76\%$ on the worst-10 tail tasks, 27.2% above ARS-LoRA with $22.5\times$ fewer parameters, while published non-ARS multi-task SAC methods report 0.0%. TOPPO matches ARS-LN-1024’s full-budget mean at $\sim 40\%$ of the 100M-step budget (Figure 1).

Summary of contributions. Our main contribution is a critic-centered diagnosis of MT-PPO failure and a stage-specific reformulation across the target, critic, and aggregation pathways.

- We diagnose three major aspects of MT-PPO critic ill-conditioning (D1–D3) and a minor aspect of actor ill-conditioning, and identify their empirical signatures in MT50 (Figures D.1 and D.3).
- We propose TOPPO, a four-module intervention (PopArt, LN-c, FairGrad ($\alpha=1$), PCGrad-a), applied at distinct stages of the per-minibatch update (Table 1 and Section 4).
- Theoretically, we show that FairGrad with $\alpha=1$ fixes the combined-gradient L^2 energy at \sqrt{K} and is invariant to positive task-wise rescaling at the aggregator output, explaining the predictable composition of PopArt and FG-c. We also introduce a projected Newton solver that makes FG-c tractable at $K=50$ (~ 50 – $1,450\times$ faster than a generic `scipy` nonlinear-solver baseline).
- We show through experiments on Meta-World+ that TOPPO outperforms existing methods, and ablations show that all four modules are needed for the full headline performance.

2 Preliminaries

We consider Markov Decision Processes (MDPs) $\{\mathcal{M}_i\}_{i=1}^K$ sharing the same state space \mathcal{S} and action space \mathcal{A} across K tasks indexed by i , with initial state $s_0 \sim \mu_i$, task-specific transition dynamics $P_i(s' | s, a)$ and reward $r_i(s, a)$ [Yu et al., 2020b, McLean et al., 2025]. In online MTRL, the agent jointly learns a task-aware policy $\pi_{\theta^a}(a | s, i)$ and state-value critic $V_{\theta^c}(s, i)$ with parameters θ^a and θ^c shared across all K tasks. The objective is to maximize the average cross-task expected discounted return $\frac{1}{K} \sum_{i=1}^K \mathbb{E}_{\pi_{\theta^a}, P_i, \mu_i}[\sum_t \gamma^t r_i(s_t, a_t)]$ with some discount factor $\gamma \in (0, 1)$.

In MT-PPO, for each task i , we collect rollouts $\{(s_t, a_t, r_i(s_t, a_t))\}$ from \mathcal{M}_i under the old policy $\pi_{\theta_{\text{old}}^a}$, then calculate the importance ratio $\rho_t^{(i)}(\theta^a) = \pi_{\theta^a}(a_t | s_t, i) / \pi_{\theta_{\text{old}}^a}(a_t | s_t, i)$, the per-task TD residual $\delta_t^{(i)} = r_i(s_t, a_t) + \gamma V_{\theta_{\text{old}}^c}(s_{t+1}, i) - V_{\theta_{\text{old}}^c}(s_t, i)$, the GAE advantage $\hat{A}_t^{(i)} = \sum_{l \geq 0} (\gamma \lambda)^l \delta_{t+l}^{(i)}$, and the return target $\hat{V}_t^{(i), \text{targ}} = \hat{A}_t^{(i)} + V_{\theta_{\text{old}}^c}(s_t, i)$ [Schulman et al., 2016]. The vanilla MT-PPO objective averages per-task losses, each combining a clipped policy surrogate, a squared value loss, and an entropy bonus [Schulman et al., 2017]:

$$\begin{aligned}
 L(\theta) &= K^{-1} \sum_{i=1}^K L_i(\theta), \quad \text{where } L_i(\theta) = L_i^a(\theta^a) + c_v L_i^c(\theta^c) - c_e H_i(\theta^a), \\
 L_i^a(\theta^a) &= -\mathbb{E}_t \left[\min(\rho_t^{(i)}(\theta^a) \hat{A}_t^{(i)}, \text{clip}(\rho_t^{(i)}(\theta^a), 1-\epsilon, 1+\epsilon) \hat{A}_t^{(i)}) \right], \\
 L_i^c(\theta^c) &= \mathbb{E}_t \left[(V_{\theta^c}(s_t, i) - \hat{V}_t^{(i), \text{targ}})^2 \right], \quad H_i(\theta^a) = \mathbb{E}_t [\mathcal{H}(\pi_{\theta^a}(\cdot | s_t, i))],
 \end{aligned} \tag{1}$$

where \mathbb{E}_t denotes the empirical average over steps in the rollout batch, $c_v, c_e > 0$ are scalar coefficients, and $\mathcal{H}(\bullet)$ is the entropy of a distribution. Per-task advantage normalization (computed within each task’s slice of a minibatch) is applied to $\hat{A}_t^{(i)}$ before the actor surrogate. This is a

task-wise variant of the per-minibatch normalization option studied in PPO implementation analyses [Andrychowicz et al., 2021]. Here it is used to remove actor-side cross-task scale differences, following the MT-PPO convention in Meta-World+ [McLean et al., 2025].

Across all K tasks, θ^a and θ^c are shared, so every gradient step must aggregate K per-task gradients over shared parameters into a single update direction. The relative magnitudes and pairwise alignment of these gradients determine whether the aggregated gradient represents the multi-task objective fairly or is dominated by a subset of tasks.

To diagnose the gradient ill-conditioning, we capture the per-task gradients $\mathbf{g}_i^a := \nabla_{\theta^a} L_i^a$ and $\mathbf{g}_i^c := \nabla_{\theta^c} L_i^c$ on the shared parameters for actor and critic, respectively. We omit global scalar coefficients such as c_v because they do not affect cross-task relative geometry. We also consider the Gram matrices $\mathbf{G}^\bullet \in \mathbb{R}^{K \times K}$, $\mathbf{G}_{ij}^\bullet = \langle \mathbf{g}_i^\bullet, \mathbf{g}_j^\bullet \rangle$ ($\bullet \in \{a, c\}$, i.e., actor and critic), where the diagonal $\mathbf{G}_{ii}^\bullet = \|\mathbf{g}_i^\bullet\|^2$ records per-task scale, and the off-diagonal cosines $\mathbf{G}_{ij}^\bullet / \sqrt{\mathbf{G}_{ii}^\bullet \mathbf{G}_{jj}^\bullet}$ record pairwise direction conflict. Throughout, we contrast each aggregator against the default average $\bar{\mathbf{g}}^\bullet = \frac{1}{K} \sum_i \mathbf{g}_i^\bullet$ applied to each shared parameter set for actor and critic.

3 Gradient Ill-conditioning

At each shared-parameter update, MT-PPO aggregates K per-task gradients into a single direction. We diagnose this aggregation along three fairness axes: preventing raw-scale domination, preserving task-specific directions, and allocating update budget according to gradient geometry rather than a few dominant tasks. Vanilla MT-PPO’s critic fails along all three axes, as summarized in Table 1 and detailed below.

- (D1) **Per-task scale spread.** Large diagonal entries \mathbf{G}_{ii}^c make the mean $\bar{\mathbf{g}}^c := K^{-1} \sum_i \mathbf{g}_i^c$ inherit the scale of high-gradient tasks, leaving small-gradient tasks with little influence.
- (D2) **Co-linear collapse.** A high mean off-diagonal $|\cos| = |\mathbf{G}_{ij}^c| / \sqrt{\mathbf{G}_{ii}^c \mathbf{G}_{jj}^c}$ for $i \neq j$ indicates that per-task critic gradients have collapsed toward a small set of shared-feature directions.
- (D3) **Unfair aggregation.** Even when scale spread and co-linearity are reduced, the default mean update can still allocate most of the combined direction to a few tasks. The aggregation rule therefore needs to be geometry-aware, not merely scale-normalized.

Critic is the dominant issue.

In our diagnostics, the per-task gradient-norm spread on the critic, $\max_i \|\mathbf{g}_i^c\| / \min_i \|\mathbf{g}_i^c\|$, is two orders of magnitude larger than the actor-side spread, $\max_i \|\mathbf{g}_i^a\| / \min_i \|\mathbf{g}_i^a\|$, and this gap persists across training (Figure 2; full diagnostics in Sections D.1 and D.3). This asymmetry is expected: per-task advantage normalization absorbs much of the reward-scale variation in the actor surrogate, whereas the critic fits unnormalized value targets unless explicitly corrected. We therefore focus the diagnosis and interventions on the critic side. Actor-side aggregation is secondary in our work, and we use PCGrad [Yu et al., 2020a] as a representative actor-gradient aggregator.

Self-reinforcing tail trap.

Early critic imbalance is damaging because it can turn small initial gaps into a self-reinforcing failure mode. In vanilla MT-PPO, the critic update averages task gradients, so the shared critic parameters θ^c are driven mainly by tasks with large critic gradients (D1–D3). Small-gradient tasks must then fit their value functions through shared features shaped primarily by other tasks’ TD errors, yielding biased advantages $\hat{A}_t^{(i)}$ and distorted actor updates. The resulting policies collect less-informative data, which further reduces useful critic signal for the same tasks in

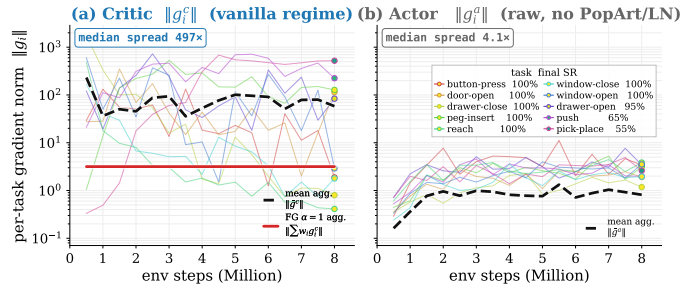


Figure 2: Per-task gradient norm for critic vs. actor in MT10 tasks from 0.5M–8.0M steps. Thin colored lines: per-task $\|\mathbf{g}_i^\bullet\|$. Overlaid bold lines: aggregated combined-gradient norm under two aggregators. (a) Critic-side: the mean aggregator $\|\bar{\mathbf{g}}^c\| = \|K^{-1} \sum_i \mathbf{g}_i^c\|$ (black dashed), the FG-c ($\alpha=1$) aggregator $\|\mathbf{d}^c\| = \|\sum_i w_i \mathbf{g}_i^c\| = \sqrt{K}$ (red) by Theorem 1. (b) Actor-side: the mean aggregator $\|\bar{\mathbf{g}}^a\| = \|K^{-1} \sum_i \mathbf{g}_i^a\|$ (black dashed).

later updates. This feedback loop explains why actor-side reweighting or gradient surgery alone gives limited gains without Critic Balancing. Empirically, vanilla MT-PPO’s worst-10 MT50 tasks average only 6.6% success at the training budget, and its five hardest tasks remain below 20% (Tables 2 and D.6). This motivates correcting critic gradient ill-conditioning early in training; see Figure 3 for *early-stage* Gram diagnostics and Figure 4 for TOPPO’s effect.

4 Method: TOPPO

To address the gradient ill-conditioning discussed in Section 3, we propose TOPPO, which consists of three critic-side modules and an actor-side gradient aggregator, listed in Table 1 and laid out in Algorithm 1.

On the critic side, **PopArt** normalizes per-task value targets, putting each task’s TD loss on the same scale before computing critic-side gradients (D1); **LN-c** (LayerNorm in the critic network) regularizes the hidden-activation conditioning that produces co-linear collapse (D2); **FG-c** ($\alpha=1$) reweights per-task gradients at the aggregator so that the pre-clipping combined-gradient norm is pinned at \sqrt{K} (D3).

On the actor side, per-task advantage normalization makes reward-scale variation much smaller, leaving direction conflict as the main residual issue. Therefore, we apply PCGrad to actor-gradient aggregation (**PCGrad-a**). Empirical comparisons with alternative actor-side aggregators are reported in Section D.1 and Table D.2.

In subsections below, we discuss the three critic-side interventions in more detail.

4.1 PopArt: per-task value-target normalization

In heterogeneous environments the per-task value-target variation can be extreme, so the squared TD loss L_i^c inherits an order-of-magnitude spread quadratically across tasks (D1).

PopArt [van Hasselt et al., 2016, Hessel et al., 2019] addresses this directly at the value-target level by inserting a per-task affine layer between the shared critic network and the value prediction. For the “Art” (Adaptively Rescaling Targets) part, the shared critic outputs a single normalized scalar $z_{\theta^c}(s, i) \in \mathbb{R}$, and a per-task scale-and-shift (σ_i, μ_i) maps it back to the raw value range by

$$V_{\theta^c}(s, i) = \sigma_i z_{\theta^c}(s, i) + \mu_i, \quad \text{where } (\mu_i, \sigma_i^2) \approx (\widehat{\mathbb{E}}_t[\widehat{V}_t^{(i), \text{targ}}], \widehat{\text{Var}}_t[\widehat{V}_t^{(i), \text{targ}}]).$$

These running estimates of each task’s target mean and variance are accumulated online via Welford’s algorithm [Welford, 1962] (canonical PopArt uses an EMA, see Section B.5). The shared critic is then trained to predict normalized per-step targets $(\widehat{V}_t^{(i), \text{targ}} - \mu_i)/\sigma_i$, which have approximately zero mean and unit variance per task by construction, so every task’s value-loss sits on the same scale.

The “Pop” (Preserving Outputs Precisely) part is a small bookkeeping step: whenever (μ_i, σ_i) update, the per-task affine head is simultaneously re-parameterized so the raw prediction $V_{\theta^c}(s, i)$ does not jump [van Hasselt et al., 2016], and the underlying critic remains a single shared MLP.

PopArt target normalization acts as a task-wise rescaling of critic gradients. Let $\mathbf{g}_i^{c, \text{PopArt}}$ be the shared-critic gradient from the PopArt-normalized critic loss, and let $\mathbf{g}_i^{c, \text{raw}}$ be the corresponding gradient from the unnormalized-target loss. For shared critic parameters θ^c and a fixed PopArt statistic σ_i during the update,

$$\mathbf{g}_i^{c, \text{PopArt}} = \sigma_i^{-2} \mathbf{g}_i^{c, \text{raw}}, \quad (2)$$

with one factor of σ_i^{-1} from the normalized residual and another σ_i^{-1} from the chain rule. This rescaling is observed empirically in Figure 3.

Algorithm 1 TOPPO: a PPO collect-and-update phase. See full version in Algorithm C.1.

Require: Tasks $\{\mathcal{M}_i\}_{i=1}^K$, $\theta = (\theta^a, \theta^c)$ with **[LN-c]** and PopArt $\{(\sigma_i, \mu_i)\}$, repeats R , max grad-norm τ

- 1: Rollout $\mathcal{B} = \bigcup_i \mathcal{B}_i$ by $\pi_{\theta_{\text{old}}^a}$; calculate $\hat{A}_t^{(i)}$, $\hat{V}_t^{(i), \text{targ}}$
- 2: **[PopArt]** update (μ_i, σ_i) , PopArt-renorm affine head
- 3: **for** $r = 1$ **to** R (recompute adv. if $r > 1$) **do**
- 4: **for** each stratified minibatch $\mathcal{B}^{\text{mb}} \subset \mathcal{B}$ **do**
- 5: normalize advantages within each task; use critic targets $(\hat{V}_t^{(i), \text{targ}} - \mu_i)/\sigma_i$ as in Section 4.1
- 6: **for** each i : compute \mathbf{g}_i^a and $\mathbf{g}_i^{c, \text{PopArt}}$ from the actor and PopArt critic losses
- 7: **[FG-c]** $\mathbf{d}^c \leftarrow \sum_i w_i \mathbf{g}_i^{c, \text{PopArt}}$ from Algorithm C.2
- 8: **[PCGrad-a]** $\mathbf{d}^a \leftarrow \text{PCGrad}(\{\mathbf{g}_i^a\})$
- 9: rescale $(\mathbf{d}^a, \mathbf{d}^c)$ by $\min(1, \tau / \|(\mathbf{d}^a, \mathbf{d}^c)\|_2)$; Adam step on θ
- 10: **end for**
- 11: **end for**

4.2 LN-c: LayerNorm on the critic network

Pre-activation LayerNorm [Ba et al., 2016] is applied to the critic’s hidden linear layers to stabilize task-wise hidden activation scales before forming \mathbf{G}^c . In early-stage critic Gram diagnostics, critic LN reduces the mean off-diagonal $|\cos|$ from 0.34 to 0.20 while roughly preserving diagonal magnitude (Figure 3; full diagnostics in Figures D.1 and D.3). This is consistent with prior RL reports on LayerNorm [Lee et al., 2025, Hansen et al., 2024]. In the MT50 cumulative ablation ladder, LN-c gives the largest single-step gain (Figure 4).

4.3 FairGrad ($\alpha=1$): per-task critic-gradient aggregation

To address unfair aggregation (D3), we replace the critic mean update with FairGrad aggregation, $\mathbf{d}^c = \sum_i w_i \mathbf{g}_i^c$, where $\mathbf{w} \in \mathbb{R}_{>0}^K$ is chosen by an α -fairness objective over task contributions [Ban and Ji, 2024].

Intuitively, FairGrad downweights tasks whose gradients already dominate the combined direction. For example, consider orthogonal gradients $\mathbf{g}_1, \mathbf{g}_2$ with norms 10 and 1, the mean direction aligns 99.5% with \mathbf{g}_1 , whereas FairGrad ($\alpha=1$) gives $w_i = 1/\|\mathbf{g}_i\|$, making the two weighted gradients have equal norms. Formally, FairGrad maximizes the α -fairness utility

$$U_\alpha(x) = \begin{cases} (1 - \alpha)^{-1} x^{1-\alpha}, & 0 < \alpha \neq 1, \\ \log x, & \alpha = 1, \end{cases} \quad (3)$$

over task contributions $x_i := (\mathbf{G}^c \mathbf{w})_i$, where x_i is task i ’s alignment with the combined direction \mathbf{d}^c . Under the standard FairGrad scaling convention, the KKT condition is $\mathbf{G}^c \mathbf{w} = \mathbf{w}^{-1/\alpha}$ componentwise. With $\alpha = 1$, the KKT condition reduces to $\mathbf{G}^c \mathbf{w} = \mathbf{w}^{-1}$. The resulting combined critic gradient has fixed L_2 norm \sqrt{K} on every minibatch and is invariant to positive task-wise rescaling $\mathbf{g}_i \mapsto c_i \mathbf{g}_i$. Formally, we have Theorem 1 below.

Theorem 1 (FairGrad ($\alpha=1$): fixed norm and scale invariance). *Let $\mathbf{g}_1, \dots, \mathbf{g}_K \in \mathbb{R}^d$ be linearly independent, with Gram matrix $\mathbf{G} = [\langle \mathbf{g}_i, \mathbf{g}_j \rangle]_{ij} \succ 0$. Let $\mathbf{w} \in \mathbb{R}_{>0}^K$ be the unique positive solution of $\mathbf{G} \mathbf{w} = \mathbf{w}^{-1}$, where the inverse is componentwise. Then $\mathbf{d} = \sum_{i=1}^K w_i \mathbf{g}_i$ has fixed norm $\|\mathbf{d}\|^2 = \mathbf{w}^\top \mathbf{G} \mathbf{w} = K$. Moreover, it is invariant to arbitrary positive rescaling. Specifically, for any $\mathbf{c} \in \mathbb{R}_{>0}^K$ and $\tilde{\mathbf{g}}_i = c_i \mathbf{g}_i$, the rescaled Gram matrix $\tilde{\mathbf{G}}$ has positive solution $\tilde{\mathbf{w}} = \mathbf{w} \odot \mathbf{c}$, and $\sum_i \tilde{w}_i \tilde{\mathbf{g}}_i = \sum_i w_i \mathbf{g}_i$. For $0 < \alpha \neq 1$, this exact scale invariance does not hold under arbitrary non-uniform \mathbf{c} . Proof is in Section C.4.*

This fixed-norm property (Theorem 1) also makes the critic update scale predictable across minibatches. Empirically, FG-c ($\alpha=1$) stabilizes the critic-to-actor combined-gradient norm ratio $\|\mathbf{d}^c\|/\|\bar{\mathbf{g}}^a\|$ during training (Figure 2), where $\bar{\mathbf{g}}^a = \frac{1}{K} \sum_i \mathbf{g}_i^a$.

Solving $\mathbf{G}^c \mathbf{w} = \mathbf{w}^{-1}$ is the main computational bottleneck for FG-c. Existing FairGrad/Nash-MTL solvers [Ban and Ji, 2024, Navon et al., 2022] are too slow for per-minibatch MT50 critic updates. The fixed-budget SGD solver in the FairGrad RL release is faster; however, it does not reliably satisfy the KKT condition (Table C.1). We therefore propose a projected Newton solver with a closed-form diagonal warm start, which reaches the target KKT tolerance with much lower wall-clock time than a generic `scipy` nonlinear-solver baseline under our implementation (see details in Section C.5).

Remark 1 (Singular Grams and solver fallbacks). Near-singular Grams \mathbf{G}^c are handled by diagonal Jacobian stabilization, diagonal warm start and logged fallbacks; see Algorithm C.2 and Section C.5.

Remark 2 (Value clipping). PPO value clipping is applied before forming \mathbf{G}^c , so clipped-out samples contribute zero to the realized minibatch gradients. We log the clip-hit fraction from this actual PPO value update, not from a counterfactual unclipped objective. This does not affect Theorem 1, which is an algebraic statement about the positive-definite Gram matrix passed to the FG-c solver.

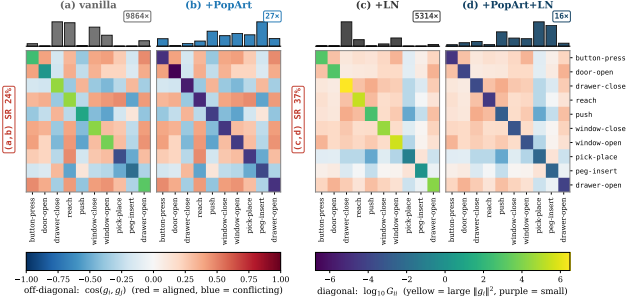


Figure 3: Early-stage ($\sim 0.5\text{M}$ steps) MT10 Gram matrices of critic gradients. Off-diagonal values are $\cos \angle(\mathbf{g}_i^c, \mathbf{g}_j^c)$ and diagonal $\log_{10} \mathbf{G}_{ii}^c$. Histograms: $\|\mathbf{g}_i^c\|/K$ and magnitude-spread ratio. See Figure D.1 for mid/late stages.

Corollary 1 (PopArt rescaling is absorbed at the FairGrad ($\alpha=1$) output). *Within one PPO mini-batch, before PopArt statistics (μ_i, σ_i) are refreshed, PopArt rescales each shared-critic gradient by $\mathbf{g}_i^{c, \text{PopArt}} = \sigma_i^{-2} \mathbf{g}_i^{c, \text{raw}}$ (Eq. (2)). If the raw critic Gram is positive definite, then by Theorem 1 the $\alpha=1$ FairGrad combined critic gradient is identical on raw and PopArt-rescaled gradients.*

Corollary 1 is an aggregator-output identity, not a trajectory-equivalence claim. It absorbs only PopArt’s multiplicative gradient-rescaling channel, not target normalization, running statistics, optimizer state, or downstream actor effects. The small PopArt marginal gain on V2 is consistent with FG-c absorbing this rescaling channel, while the V1 ablation in Section 5.3 shows that PopArt’s non-rescaling effects can still matter.

5 Experiments

5.1 Setup

Benchmark. We train and evaluate all models on Meta-World V2 [Yu et al., 2020b, McLean et al., 2025], MT10 ($K=10$) and MT50 ($K=50$) over all tasks with a task identifier. We use V2 reward throughout the paper unless specifically labeled V1.

Architecture. TOPPO, our PPO-based method, adopts a fully task-shared $[400 \times 3]$ ReLU MLP, the standard Meta-World multi-task backbone adopted by most prior works, including the SAC-family in Meta-World+ [McLean et al., 2025] and the structured-RL methods CAGrad / CARE / PaCo / MOORE / FAMO / FairGrad, with separate actor and critic of the same size. The only per-task structure is the input one-hot and the action log standard deviation σ_i . ARS [Cho et al., 2025] uses architectures with deeper $[400 \times 4]$ MLPs by default, and wider $[1024 \times 4]$ MLPs for ARS-LN-1024 (a scaled version). Our TOPPO has 685K (MT10) / 717K (MT50) parameters, which are 22.5–22.7× smaller than the strongest ARS variants (See Table B.2 and Section B.1).

Training. Our models are trained with 20M (MT10) / 100M (MT50) total environment steps (2M per task), matching the ARS / MOORE / PaCo / Meta-World+ convention. Our TOPPO *headline* configuration is PCGrad-a + FG-c ($\alpha=1$) + PopArt + LN-c; the *vanilla MT-PPO* baseline removes all four interventions while retaining standard MT-PPO machinery (per-task advantage normalization, stratified minibatches, value clip, post-aggregation $\|\cdot\| \leq 1$ clip), so the contrast isolates the four interventions. Full hyperparameters are in Table B.1; PPO-specific adaptations of SAC-based gradient-surgery methods are in Section B.4.

Baselines and reporting. For comparability, each comparison keeps the reward version and reporting statistic fixed. For V2 reward, baseline rows are from Tables 1 and 2 of Cho et al. [2025]. We follow the same final-checkpoint mean \pm standard deviation (std) protocol, using 10 seeds for our rows versus 8 in the published baselines. For the V1 head-to-head with Meta-World+ [McLean et al., 2025], both our rows and the baseline rows follow the Meta-World+ 10-seed final-checkpoint Interquartile Mean (IQM) \pm std (Table 3). Baseline provenance, step budgets, protocol differences, 4-metric disclosure, and per-task success rates are audited in Sections B.3 and D.6 and Tables D.8 to D.10.

Code and reproducibility. Code Repository: To be released.

5.2 Main Results

MT50 mean and Worst- k tail tasks. On MT50, TOPPO beats the strongest published baseline on both ends of the metric: 1.98% \uparrow on the mean vs. ARS-LN-1024 at 22.7× fewer parameters (Table 2), and 27.2% \uparrow on the worst-10 tail tasks vs. ARS-LoRA at 22.5× fewer parameters (Table 2). All published non-ARS multi-task SAC methods score 0.0% on the worst-10 tail tasks.

MT10: every seed clears 99%, the final-vs-best gap is oscillation. The MT10 *final*-checkpoint mean success rate in Table 2 sits a few percent below ARS-LoRA, but every seed in fact reaches $\geq 99\%$ at its own best checkpoint (see per-seed best columns in Table D.10). This gap reflects PPO’s

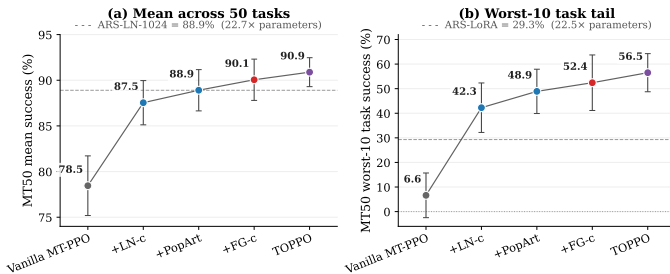


Figure 4: MT50 ablation ladder. (a) Final mean. (b) Final worst-10 tail tasks. $n=10$ seeds, \pm std; dashed lines mark the strongest published baseline for each metric.

Table 2: Meta-World V2 headline success rate and Worst- k tail tasks. Values are final-checkpoint success rates (%); gray entries are std where available. “–” denotes source-unpublished entries.

Algorithm	MT10		MT50						
	Params	Success rate %	Params	Worst- k tail-tasks success rate (%)					
				$k=5$	$k=10$	$k=20$	$k=30$	$k=40$	$k=50$ (All)
SAC-MT	2517K	69.4 ± 0.8	2597K	0.0 ± 0.0	0.0 ± 0.0	0.0 ± 0.0	14.1 ± 3.1	34.5 ± 2.5	47.6 ± 2.0
MT-MH-SAC	2546K	77.2 ± 11.9	2754K	0.0 ± 0.0	0.0 ± 0.0	0.0 ± 0.0	14.1 ± 1.7	34.0 ± 2.0	47.2 ± 1.7
Soft Modularization	3454K	74.4 ± 10.5	3534K	0.0 ± 0.0	0.0 ± 0.0	1.8 ± 3.7	23.7 ± 12.3	42.6 ± 9.5	54.1 ± 7.6
PCGrad-SAC	2517K	74.8 ± 13.7	2597K	0.0 ± 0.0	0.0 ± 0.0	0.0 ± 0.0	21.0 ± 12.9	39.9 ± 10.7	51.9 ± 8.5
PaCo	–	82.4 ± 14.2	–	0.0 ± 0.0	0.0 ± 0.0	4.6 ± 8.2	26.1 ± 15.0	44.6 ± 11.2	55.6 ± 9.1
MOORE	6890K	86.0 ± 4.8	7403K	0.0 ± 0.0	0.0 ± 0.0	15.9 ± 7.0	41.2 ± 5.0	55.3 ± 3.9	64.2 ± 3.1
SMT	–	86.8 ± 8.6	–	0.0 ± 0.0	0.0 ± 0.0	8.0 ± 8.9	26.8 ± 13.1	45.0 ± 9.9	56.0 ± 8.0
ARS	2517K	97.3 ± 2.1	2597K	–	9.1 ± 6.6	26.3 ± 6.1	45.3 ± 4.7	57.5 ± 3.6	65.9 ± 2.9
ARS-LN (400)	2530K	98.6 ± 1.5	2611K	–	21.0 ± 11.4	49.1 ± 6.5	64.3 ± 6.2	72.9 ± 4.7	78.3 ± 3.7
ARS-LN (1024)	–	–	16267K	–	–	–	–	–	88.9 ± 2.6
ARS-LoRA	3878K	99.5 ± 0.8	16123K	–	29.3 ± 7.7	58.4 ± 4.5	72.0 ± 3.0	79.0 ± 2.2	83.2 ± 1.8
Ours: Vanilla MT-PPO	684K	85.2 ± 6.5	716K	0.0 ± 0.0	6.6 ± 9.1	46.3 ± 8.0	64.1 ± 5.4	73.1 ± 4.1	78.5 ± 3.3
+LN-c	685K	96.2 ± 3.4	717K	6.9 ± 11.4	42.3 ± 10.1	68.9 ± 5.9	79.2 ± 4.0	84.4 ± 3.0	87.5 ± 2.4
+LN-c +PopArt	685K	96.8 ± 1.5	717K	18.0 ± 12.5	48.9 ± 9.0	72.3 ± 5.6	81.5 ± 3.8	86.1 ± 2.8	88.9 ± 2.3
+LN-c +PopArt +FG-c	685K	94.8 ± 5.1	717K	22.3 ± 17.3	52.4 ± 11.3	75.1 ± 5.7	83.4 ± 3.8	87.6 ± 2.8	90.1 ± 2.3
TOPPO	685K	97.2 ± 3.1	717K	24.2 ± 14.1	56.5 ± 7.8	77.2 ± 4.0	84.8 ± 2.6	88.6 ± 2.0	90.9 ± 1.6

well-known late-training instability, for which linear learning-rate annealing is a documented code-level practice [Engstrom et al., 2020, Andrychowicz et al., 2021]. To obtain an *honest comparison*, we *deliberately do not* apply such a learning rate schedule, to keep training-time hyperparameters *identical* across all our configurations and align with the published-baseline protocol that reports a single fixed-schedule final-checkpoint number. We report *final* as the headline statistic as it is the most conservative and matches the protocol used in most published baselines (see Table D.9). For more detailed results, see per-seed argmax-step distribution and the full 4-metric breakdown in Tables D.10 and D.11.

Cumulative ladder. Figure 4 traces how the four intervention effects accumulate on MT50. Vanilla MT-PPO with LN-c and PopArt already reaches mean parity with ARS-LN-1024 and exceeds ARS-LoRA on the worst-10 tail tasks. Modules FG-c ($\alpha=1$) and PCGrad-a then add mechanism-aligned residual gains. Adding LN-c is the largest single jump on both metrics. Note that this effect ladder is just a path-wise description, not a unique additive decomposition, as the 3 critic interventions interact (Corollary 1 and Section 5.3).

Convergence speed and parameter efficiency. On MT50, Figure 1a shows TOPPO crossing every published baseline’s 100M-step final mean within $\sim 40\%$ of its own training budget, the slowest crossing (ARS-LN-1024) at ~ 40 M steps; ARS-LoRA at ~ 23 M, ARS-LN-400 at ~ 18 M, MOORE at ~ 11 M. With $22.7\times$ fewer parameters than ARS-LN-1024, TOPPO sits on the parameter and sample efficiency frontier among the compared V2 methods despite being on-policy.

5.3 Ablation and analysis

We isolate each component’s contribution via three ablations. Full details are in Section D.1.

Critic-side intervention cube (LN-c \times PopArt \times FG-c, 8 cells \times 10 seeds, MT50 V2). Each component is mechanism-distinct and they interact. The interaction signature suggested by Corollary 1 appears at training-outcome scale: *PopArt’s worst-10 marginal collapses from 6.64% \uparrow (over LN-c) to 0.22% \downarrow (over LN-c+FG-c)*. This is consistent with FairGrad ($\alpha=1$) absorbing PopArt’s per-task gradient rescaling at the gradient aggregator (Table D.1).

Per-side combiner asymmetry. Actor-side scale spread is small after per-task advantage normalization, leaving direction conflict as the main residual issue (Figure 2). This motivates our PCGrad-a/FG-c asymmetric design: PCGrad-a stabilizes worst-10 tail-tasks seed std from 11.29% to 7.76% (Table 2); FG-a on top of FG-c underperforms default-actor FG-c (89.2% vs. 90.0%, Table D.2). FG-c vs. PCGrad-c is a tie within seed noise. We adopt FG-c on the critic for the \sqrt{K} -energy identity and scale-invariance of Theorem 1 (see all per-side combiners in Section C.3).

V1 reward sensitivity. PopArt’s non-rescaling channels (running statistics, Adam moments, downstream actor) are predicted to become individually load-bearing under per-task heterogeneous reward

Table 3: Meta-World V1 (MT50): TOPPO vs. Meta-World+ baselines. Values are final-checkpoint IQM \pm std (10 seeds). Top: our V1 ablation; bottom: published V1 baselines.

Method	Params	Success rate %	TOPPO step to match	Backbone
Ours: Vanilla MT-PPO	716K	45.2 \pm 2.4	–	[400] \times 3
+LN-c	717K	64.3 \pm 3.1	–	[400] \times 3
+LN-c +FG-c	717K	62.0 \pm 2.7	–	[400] \times 3
+LN-c +PopArt	717K	76.5 \pm 2.0	–	[400] \times 3
+LN-c +PopArt +FG-c	717K	79.0 \pm 1.2	–	[400] \times 3
TOPPO	717K	79.3 \pm 1.3	–	[400] \times 3
<i>Meta-World+ MT50 SAC-family V1 baselines [McLean et al., 2025]</i>				
MT-MH-SAC	2031K	31.9 \pm 2.7	\sim 3.4M (3%)	[400] \times 3 shared, per-task heads
Soft Modularization	8030K	60.6 \pm 3.9	\sim 12M (12%)	routing [256] \times 4 \times 4
MOORE	10385K	61.8 \pm 2.7	\sim 13M (13%)	[400] \times 3, 6 experts
PaCo	33909K	18.6 \pm 15.4	\sim 2.1M (2%)	[400] \times 3, $K=20$
PCGrad-SAC	2031K	45.8 \pm 5.9	\sim 5.5M (5%)	[400] \times 3 shared, per-task heads

scales. In the MT50 V1 sweep (Section D.5 and Table 3), the PopArt marginal over LN-c+FG-c is 17.01% \uparrow on IQM (vs. 0.32% \uparrow on V2 IQM, Table D.3) and over LN-c (no FG-c) is 12.26% \uparrow (vs. 1.35% \uparrow on V2 IQM). The V2 collapse signature predicted by Corollary 1 is therefore inverted on V1: only the per-task gradient rescaling channel is absorbed by FG-c, while the others are not. Equivalently, the V1 ladder has a different shape: PopArt rather than LN-c is the largest single step, and FG-c without PopArt slightly hurts (2.29% \downarrow over LN-c on V1 IQM, vs. 1.68% \uparrow on V2 IQM).

V1 head-to-head with external baselines. Beyond mechanism, the same V1 sweep set against the Meta-World+ MT50 SAC-family baselines on V1 (Table 3, both panels reported under the Meta-World+ IQM \pm std convention) shows TOPPO IQM at 79.3%, 17.6% \uparrow vs. the strongest published V1 baseline (MOORE, 61.8%) at 14.5 \times fewer trainable parameters (717K vs. 10,385K); SAC-PCGrad on V1 lands 33.5% \downarrow vs. TOPPO. The fully stacked TOPPO row remains the strongest configuration, but the V1 ladder differs from V2 in the way described above, with PopArt becoming more important under heterogeneous rewards.

Limitations. We do not claim empirical dominance of FG-c over all critic-side combiners: FG-c and PCGrad-c are tied within seed noise under LN-c+PopArt, and we adopt FG-c for the mechanism property of Theorem 1. We also did not exhaustively test actor-side aggregator choices beyond the per-side cube in Table D.2. Therefore, PCGrad-a should be read as a mechanism-aligned working choice rather than an optimal actor combiner. Our reported architecture also uses separate actor and critic networks; if an actor–critic model uses a shared feature extractor before branching into policy and value heads, assigning critic-side balancing and actor-side surgery on the shared parameters becomes a coupled design choice that requires separate study. Our PopArt uses Welford full-history sample statistics rather than the canonical EMA (Section B.5). Under non-stationary RL returns, the canonical EMA may be better suited. Empirically, the two estimators are numerically closest during the early-training phase that decides the self-reinforcing tail-trap (Section B.5), suggesting that the estimator choice is less likely to determine the headline outcome.

6 Conclusion

We rethink PPO for MTRL under a vanilla shared MLP. Our results show that earlier conclusions drawn from MT-PPO’s \sim 30% MT10 success rate in the original Meta-World benchmark [Yu et al., 2020b] underestimated PPO by confounding the choice of optimizer family with the condition of the critic. We identify critic-side gradient ill-conditioning as the main failure mode: large per-task scale spread, representation-level co-linear collapse, and unfair aggregation of imbalanced gradients. TOPPO targets these failures with PopArt, critic LayerNorm, and critic-side FairGrad ($\alpha=1$), linked by the scale-invariance result of Theorem 1 and Corollary 1. With only 717K parameters, TOPPO reaches 90.88 \pm 1.59% MT50 final mean and 56.50 \pm 7.76% on the worst-10 tail tasks, while matching ARS-LN-1024’s full-budget mean at \sim 40% of the training budget. MT-PPO’s tail-task recovery therefore comes from critic-side gradient intervention rather than architectural complexity.

References

- Marcin Andrychowicz, Anton Raichuk, Piotr Stańczyk, Manu Orsini, Sertan Girgin, Raphaël Marinier, Léonard Hussenot, Matthieu Geist, Olivier Pietquin, Marcin Michalski, Sylvain Gelly, and Olivier Bachem. What matters for on-policy deep actor-critic methods? a large-scale study. In *International Conference on Learning Representations*, 2021. arXiv:2006.05990.
- Jimmy Lei Ba, Jamie Ryan Kiros, and Geoffrey E. Hinton. Layer normalization. *arXiv preprint arXiv:1607.06450*, 2016.
- Hao Ban and Kaiyi Ji. Fair resource allocation in multi-task learning. In *Proceedings of the 41st International Conference on Machine Learning*, volume 235 of *Proceedings of Machine Learning Research*, pages 2715–2731. PMLR, 2024. arXiv:2402.15638.
- Tony F. Chan, Gene H. Golub, and Randall J. LeVeque. Algorithms for computing the sample variance: Analysis and recommendations. *The American Statistician*, 37(3):242–247, 1983. doi: 10.1080/00031305.1983.10483115.
- Zhao Chen, Vijay Badrinarayanan, Chen-Yu Lee, and Andrew Rabinovich. GradNorm: Gradient normalization for adaptive loss balancing in deep multitask networks. In *Proceedings of the 35th International Conference on Machine Learning*, volume 80 of *Proceedings of Machine Learning Research*, pages 794–803. PMLR, 2018.
- Myungsik Cho, Jongeui Park, Jeonghye Kim, and Youngchul Sung. ARS: Adaptive reward scaling for multi-task reinforcement learning. In *Proceedings of the 42nd International Conference on Machine Learning*, volume 267 of *Proceedings of Machine Learning Research*. PMLR, 2025. OpenReview id U0mI6M7lvI; code at <https://github.com/ms-cho/Adaptive-Reward-Scaling-ARS-for-MTRL>.
- Logan Engstrom, Andrew Ilyas, Shibani Santurkar, Dimitris Tsipras, Firdaus Janoos, Larry Rudolph, and Aleksander Madry. Implementation matters in deep policy gradients: A case study on PPO and TRPO. In *International Conference on Learning Representations*, 2020. arXiv:2005.12729.
- Tuomas Haarnoja, Aurick Zhou, Pieter Abbeel, and Sergey Levine. Soft actor-critic: Off-policy maximum entropy deep reinforcement learning with a stochastic actor. In *Proceedings of the 35th International Conference on Machine Learning*, volume 80 of *Proceedings of Machine Learning Research*, pages 1861–1870. PMLR, 2018.
- Nicklas Hansen, Hao Su, and Xiaolong Wang. TD-MPC2: Scalable, robust world models for continuous control. In *International Conference on Learning Representations*, 2024. arXiv:2310.16828.
- Ahmed Hendawy, Jan Peters, and Carlo D’Eramo. Multi-task reinforcement learning with mixture of orthogonal experts. In *International Conference on Learning Representations*, 2024. arXiv:2311.11385.
- Matteo Hessel, Hubert Soyer, Lasse Espeholt, Wojciech Czarnecki, Simon Schmitt, and Hado van Hasselt. Multi-task deep reinforcement learning with PopArt. In *Proceedings of the AAAI Conference on Artificial Intelligence*, volume 33, pages 3796–3803, 2019. arXiv:1809.04474.
- Viraj Joshi, Zifan Xu, Bo Liu, Peter Stone, and Amy Zhang. Benchmarking massively parallelized multi-task reinforcement learning for robotics tasks. *Reinforcement Learning Journal*, 2025. arXiv:2507.23172; presented at the Reinforcement Learning Conference (RLC) 2025.
- Frank P. Kelly. Charging and rate control for elastic traffic. *European Transactions on Telecommunications*, 8(1):33–37, 1997.
- Alex Kendall, Yarin Gal, and Roberto Cipolla. Multi-task learning using uncertainty to weigh losses for scene geometry and semantics. In *IEEE Conference on Computer Vision and Pattern Recognition*, pages 7482–7491, 2018.
- Vitaly Kurin, Alessandro De Palma, Ilya Kostrikov, Shimon Whiteson, and M. Pawan Kumar. In defense of the unitary scalarization for deep multi-task learning. In *Advances in Neural Information Processing Systems*, 2022.

- Hoon Lee, Dongyoon Hwang, Donghu Kim, Hyunseung Kim, Jun Jet Tai, Kaushik Subramanian, Peter R. Wurman, Jaegul Choo, Peter Stone, and Takuma Seno. SimBa: Simplicity bias for scaling up parameters in deep reinforcement learning. In *International Conference on Learning Representations*, 2025. arXiv:2410.09754.
- Bo Liu, Xingchao Liu, Xiaojie Jin, Peter Stone, and Qiang Liu. Conflict-averse gradient descent for multi-task learning. In *Advances in Neural Information Processing Systems*, volume 34, 2021.
- Bo Liu, Yihao Feng, Peter Stone, and Qiang Liu. FAMO: Fast adaptive multitask optimization. In *Advances in Neural Information Processing Systems*, 2023. arXiv:2306.03792.
- Shikun Liu, Edward Johns, and Andrew J. Davison. End-to-end multi-task learning with attention. In *IEEE Conference on Computer Vision and Pattern Recognition*, pages 1871–1880, 2019.
- Reginald McLean, Evangelos Chatzaroulas, Luc McCutcheon, Frank Röder, Tianhe Yu, Zhanpeng He, K.R. Zentner, Ryan Julian, J K Terry, Isaac Woungang, Nariman Farsad, and Pablo Samuel Castro. Meta-world+: An improved, standardized, RL benchmark. In *Advances in Neural Information Processing Systems Datasets and Benchmarks Track*, 2025. arXiv:2505.11289.
- Jeonghoon Mo and Jean Walrand. Fair end-to-end window-based congestion control. *IEEE/ACM Transactions on Networking*, 8(5):556–567, 2000.
- John F. Nash. The bargaining problem. *Econometrica*, 18(2):155–162, 1950.
- Aviv Navon, Aviv Shamsian, Idan Achituve, Haggai Maron, Kenji Kawaguchi, Gal Chechik, and Ethan Fetaya. Multi-task learning as a bargaining game. In *Proceedings of the 39th International Conference on Machine Learning*, volume 162 of *Proceedings of Machine Learning Research*, pages 16428–16446. PMLR, 2022.
- John Schulman, Philipp Moritz, Sergey Levine, Michael Jordan, and Pieter Abbeel. High-dimensional continuous control using generalized advantage estimation. In *International Conference on Learning Representations*, 2016. arXiv:1506.02438.
- John Schulman, Filip Wolski, Prafulla Dhariwal, Alec Radford, and Oleg Klimov. Proximal policy optimization algorithms. *arXiv preprint arXiv:1707.06347*, 2017.
- Shagun Sodhani, Amy Zhang, and Joelle Pineau. Multi-task reinforcement learning with context-based representations. In *Proceedings of the 38th International Conference on Machine Learning*, volume 139 of *Proceedings of Machine Learning Research*, pages 9767–9779. PMLR, 2021. arXiv:2102.06177.
- Lingfeng Sun, Haichao Zhang, Wei Xu, and Masayoshi Tomizuka. PaCo: Parameter-compositional multi-task reinforcement learning. In *Advances in Neural Information Processing Systems*, volume 35, 2022. arXiv:2210.11653.
- Hado P. van Hasselt, Arthur Guez, Matteo Hessel, Volodymyr Mnih, and David Silver. Learning values across many orders of magnitude. In *Advances in Neural Information Processing Systems*, volume 29, 2016. arXiv:1602.07714.
- B. P. Welford. Note on a method for calculating corrected sums of squares and products. *Technometrics*, 4(3):419–420, 1962. doi: 10.1080/00401706.1962.10490022.
- Ruihan Yang, Huazhe Xu, Yi Wu, and Xiaolong Wang. Multi-task reinforcement learning with soft modularization. In *Advances in Neural Information Processing Systems*, volume 33, 2020. arXiv:2003.13661.
- Tianhe Yu, Saurabh Kumar, Abhishek Gupta, Sergey Levine, Karol Hausman, and Chelsea Finn. Gradient surgery for multi-task learning. In *Advances in Neural Information Processing Systems*, volume 33, 2020a.
- Tianhe Yu, Deirdre Quillen, Zhanpeng He, Ryan Julian, Karol Hausman, Chelsea Finn, and Sergey Levine. Meta-world: A benchmark and evaluation for multi-task and meta reinforcement learning. In *Proceedings of the Conference on Robot Learning*, volume 100 of *Proceedings of Machine Learning Research*, pages 1094–1100. PMLR, 2020b. arXiv:1910.10897.

Appendix Contents

A	Extended Related Work	12
B	Implementation Details	13
B.1	Detailed experimental setup	13
B.2	Hyperparameters and architecture	14
B.3	Parameter audit (source-counted)	15
B.4	PPO-specific adaptations of SAC-based gradient-surgery methods	16
B.5	PopArt: implementation note (Welford full-sample statistics)	17
C	Theoretical Details	18
C.1	TOPPO pseudocode	18
C.2	α -fairness family and KKT derivation	18
C.3	Aggregator family taxonomy and cone containment	19
C.4	Proof of Theorem 1 (scale invariance)	20
C.5	y -Newton solver derivation and benchmark protocol	21
D	Additional Experimental Results	23
D.1	Detailed ablation results	23
D.2	Diagnostic dump-run provenance	25
D.3	Mechanism evidence figures	25
D.4	Headline V2 learning curves	28
D.5	V1 reward sensitivity	29
D.6	Per-task success rates	31
D.7	Cross-paper reporting-protocol map	37

A Extended Related Work

Structure-based multi-task RL. Architectural interventions form one line of multi-task RL: Soft Modularization [Yang et al., 2020], CARE [Sodhani et al., 2021], PaCo [Sun et al., 2022], and MOORE [Hendawy et al., 2024]. The original Meta-World paper [Yu et al., 2020b] reported MT-PPO at $\sim 30\%$ on MT10, anchoring a community shift to SAC backbones for subsequent multi-task RL methods (CARE, PaCo, MOORE, PCGrad-SAC, ARS [Cho et al., 2025]); benchmarks have largely standardized on the SAC stack [McLean et al., 2025]. We hold the architecture fixed at a vanilla shared MLP and revisit the SAC-PPO comparison at this constant architecture. Concurrent work [Joshi et al., 2025] observes via cross-task gradient cosine that conflicts dominate on the critic in MT-PPO and bypasses the critic via Monte-Carlo returns, whereas we diagnose a complementary scale-imbalance axis ($497\times$ vs. $4.1\times$ per-task norm spread) and fix the critic at the three layers above.

Imbalance interventions across pipeline layers. *Per-task gradient aggregation:* scalar-signal reweighting (loss-level: uncertainty weighting [Kendall et al., 2018], DWA [Liu et al., 2019], FAMO [Liu et al., 2023]; per-task gradient-norm: GradNorm [Chen et al., 2018]) is Gram-blind;

direction surgery uses Gram inner products (PCGrad [Yu et al., 2020a], CAGrad [Liu et al., 2021]); α -fairness reweighting solves $\mathbf{G}\mathbf{w} = \mathbf{w}^{-1/\alpha}$ on the full Gram (FairGrad [Ban and Ji, 2024]; at $\alpha=1$ equivalent to Nash bargaining [Navon et al., 2022], Remark C.1). Kurin et al. [2022] argue that across supervised MTL benchmarks and Meta-World multi-task SAC, the simple uniform sum of losses (unitary scalarization) matches specialized multi-task optimizers once standard regularization is matched; our diagnostic evidence (Figure 2: critic per-task gradient-norm spread $497\times$) is on MT-PPO specifically, a regime they do not test, where loss-level signals provably cannot recover the per-task gradient rescaling FairGrad ($\alpha=1$) absorbs (Theorem 1 and Corollary 1). The Kurin SAC result is consistent with our PopArt-removed ablations on V1 (which has wider per-task return scale heterogeneity, Table D.3) showing that direction-only loss-level signals fall short once the critic-side per-task scale spread is load-bearing. Section C.3 positions these methods as different points in the same shared cone $\text{cone}^+\{\mathbf{g}_i\}$; only FairGrad ($\alpha=1$) carries the scale-invariance of Theorem 1 that links it to PopArt via Corollary 1. *Value-target normalization* (PopArt [van Hasselt et al., 2016, Hessel et al., 2019]; ARS rescales the per-task reward fed into the Bellman target [Cho et al., 2025]) and *representation regularization* (LayerNorm [Ba et al., 2016], applied in deep RL by [Lee et al., 2025, Hansen et al., 2024]) are standard; Corollary 1 restricts the new PopArt \rightarrow FG-c content to PopArt’s per-task gradient-rescaling effect $c_i = \sigma_i^{-2}$.

B Implementation Details

B.1 Detailed experimental setup

This appendix expands the main-text Section 5.1 with the full benchmark, architecture, training, and evaluation description; hyperparameter values are tabulated in Table B.1 (Section B.2), PPO-specific adaptations of SAC-based gradient-surgery methods are documented in Section B.4, the source-counted parameter audit against published baselines is in Section B.3, and cross-paper protocol differences are mapped in Section D.7.

Benchmark and observations. We use Meta-World 3.0.0 [Yu et al., 2020b, McLean et al., 2025] with V2 reward semantics throughout the paper unless explicitly labeled V1. The K tasks (reaching, picking, pushing, opening doors, peg-insertion, etc.) share the same continuous observation space \mathcal{S} and continuous action space \mathcal{A} ; what varies across tasks is the reward function and the dynamics. The agent receives the state concatenated with a one-hot task identifier of length K as input, and is trained on all K tasks simultaneously via stratified minibatches. Meta-World offers two reward variants: V1 is the original per-task reward set from Yu et al. [2020b] with substantial per-task scale heterogeneity, while V2 [McLean et al., 2025] redesigns the per-task rewards with PPO solvability and comparable per-task scales as explicit design criteria. We evaluate TOPPO on *both* variants: on the load-bearing MT50 benchmark it outperforms the strongest matched-protocol published baseline under both V2 mean/worst- k reporting and V1 IQM reporting, demonstrating robustness across the V1/V2 reward redesign rather than dependence on V2’s scale rebalancing. V2 carries the headline (MT50 V2 is the main number; MT10 V2 saturates near-ceiling under any reasonable critic-side intervention and is reported for completeness, Section 5.2); V1 is the sensitivity sweep that also tests Corollary 1’s scope under heterogeneous per-task return scales (Section D.5).

Architecture. Actor and critic are separate networks of identical [400, 400, 400] shape (full architecture in Table B.1); this is the standard SAC-family Meta-World+ backbone used by CAGrad [Liu et al., 2021], CARE [Sodhani et al., 2021], PaCo [Sun et al., 2022], MOORE [Hendawy et al., 2024], FAMO [Liu et al., 2023], and FairGrad [Ban and Ji, 2024], while ARS [Cho et al., 2025] is the architectural outlier with a deeper [400 \times 4] default or a wider [1024 \times 4] ARS-LN-1024 variant. The only per-task structure consists of the one-hot task identifier in the input and an $|\mathcal{A}|$ -dimensional per-task log-stddev σ_i for the diagonal-Gaussian action distribution; there are no per-task output heads, expert mixtures, LoRA adapters, modular routers, or task-specific subnetworks. Headline parameter counts are 685K (MT10) and 717K (MT50); per-component breakdowns and ratios against published baselines are tabulated in Table B.2 (Section B.3).

Training pipeline. Stratified minibatch sampling guarantees the per-task gradients $\mathbf{g}_i^a, \mathbf{g}_i^c$ on the shared parameters are well-defined every minibatch. Per-task advantage normalization (zero-mean unit-variance computed within each task’s slice of a minibatch) is applied before the actor surrogate;

this task-wise adaptation of a PPO implementation option is the actor-side mechanism that drives the actor-critic asymmetry diagnosed in Section 3. We retain PPO’s value clip and apply a post-aggregation gradient-norm clip uniformly across all configurations. Full numerical hyperparameter values are in Table B.1; PPO-specific adaptations made when porting SAC-based gradient-surgery methods (PCGrad, CAGrad, FairGrad) to PPO are documented in Section B.4.

Evaluation protocol. All numbers reported in the paper come from *evaluation* rollouts under the deterministic policy mean (no exploration noise), not training rollouts. Following the Meta-World convention [Yu et al., 2020b, McLean et al., 2025], at each evaluation checkpoint the agent is rolled out once per training goal position per task: 50 goal positions \times K tasks = 500 episodes per evaluation on MT10 and 2,500 on MT50. A per-task “success rate” is the fraction of those episodes whose success flag is 1 at *any* step during the episode (the default Meta-World success criterion inherited from the benchmark code, not a termination-only criterion); the reported scalar is the cross-task mean of per-task success rates.

Reporting choices. We run 10 seeds and report final-checkpoint success rates. To match each baseline’s published convention, we report mean \pm std against the V2 baselines from Cho et al. [2025] (Table 2) and IQM \pm std against the Meta-World+ V1 baselines (Table 3); for our rows, both views are computed from the same 10-seed run set. The full 4-metric breakdown of every reported configuration is in Table D.10, cross-paper convention conversions are in Section D.7, and per-task breakdowns are in Section D.6.

Compute resources. TOPPO is trained on a single NVIDIA RTX 3090 GPU with 16 CPU cores and 64 GB memory per run; one MT10 seed (20M environment steps) takes \sim 6 hours and one MT50 seed (100M environment steps) takes \sim 24 hours of wall-clock time. These figures cover the full 20M/100M-step training budget (matching the published-baseline convention) and include 51 evaluation checkpoints performed during training (one every 2 epochs across the 100 training epochs, plus one at initialization); pure training time without evaluation is shorter. TOPPO already converges to strong performance well before the full budget is exhausted (Section 5.2 and Figure 1); the full schedule is reported to match the published reporting protocol, while shorter runs can be sufficient when strict final-checkpoint comparability is not required.

B.2 Hyperparameters and architecture

Inherited from Meta-World+. The PPO numerical hyperparameters in Table B.1 (loss coefficients, GAE λ , clip range, learning rate, PPO repeats per collect, minibatch count, gradient-norm clip, MLP backbone, per-rollback step counts and total environment-step budgets) are inherited verbatim from the Meta-World+ companion repository [McLean et al., 2025] (<https://github.com/rainx0r/metaworld-algorithms>); we do not separately tune any of these values. The one substantive deviation from their MT50 example config is that we keep value clipping on (their MT50 example disables it). Per-task advantage normalization and stratified minibatch sampling are PPO-side multi-task adaptations on top of this baseline (Section B.4); FairGrad / PCGrad / CAGrad / PopArt / LayerNorm hyperparameters are listed under their respective entries below.

Table B.1: Production hyperparameters for the experiments in Section 5. The three FairGrad solver entries below the per-side α rows (y_{\max} , η , max Newton iters) are fixed solver constants, not swept.

Parameter	MT10	MT50
<i>Network architecture (fully task-shared except per-task σ)</i>		
actor θ^a hidden sizes	[400, 400, 400]	[400, 400, 400]
actor output projection	shared Linear(400, $ \mathcal{A} $) for μ	shared Linear(400, $ \mathcal{A} $) for μ
critic θ^c hidden sizes	[400, 400, 400]	[400, 400, 400]
critic output projection	shared Linear(400, 1) for V	shared Linear(400, 1) for V
per-task log-stddev σ_i	$ \mathcal{A} $ params per task	$ \mathcal{A} $ params per task
task identity input	one-hot, length $K = 10$	one-hot, length $K = 50$
activation	ReLU	ReLU
LayerNorm placement (TOPPO)	critic hidden layers only	critic hidden layers only
<i>Training</i>		
epochs	100	100
env steps per epoch	200,000	1,000,000
env steps per collect	100,000	500,000
PPO repeats per collect	16	16
minibatch size (= step/32)	3,125	15,625
minibatch sampling	stratified	stratified
learning rate (Adam)	3×10^{-4}	3×10^{-4}
max gradient norm (post-aggregation)	1.0	1.0
discount γ	0.99	0.99
<i>PPO</i>		
GAE λ	0.97	0.97
clip range ϵ	0.2	0.2
value clip	enabled	enabled
value loss weight c_v	0.001	0.001
entropy bonus c_e	0.005	0.005
per-task advantage normalization	enabled	enabled
recompute advantage per repeat	enabled	enabled
<i>FairGrad (when active)</i>		
actor α_a	2.0	2.0
critic α_c	1.0	1.0
solver y-cap y_{\max}	50	50
solver Newton tol η	10^{-2}	10^{-2}
solver max Newton iters	50	50
<i>Evaluation</i>		
eval episodes per task	50	50
seeds reported	10	10

LayerNorm placement notes.

- Pre-activation LN on hidden Linear layers of critic network only; actor hidden layers are LN-free.
- SimBa/TD-MPC2-style symmetric LN [Lee et al., 2025, Hansen et al., 2024] (LN on both actor and critic hidden layers) is the natural baseline; TOPPO deliberately uses critic-only LN. The symmetric-LN ablation is discussed with the intervention results in Section D.1.
- LN-enabled critic hidden Linear uses bias=False (LN’s mean subtraction makes bias mathematically redundant); critic output projection retains its bias.

B.3 Parameter audit (source-counted)

Convention. Throughout the paper, every “parameter count” refers to the *total number of parameters held in memory during training, excluding optimizer state* — exactly the quantity that determines the GPU footprint of a method. For our PPO this is just actor + critic (no target network). For SAC-style baselines this is actor + $2 \times$ critic + $2 \times$ target_critic + α , where the twin Q-critics are stacked on a num_critics=2 axis and the Polyak-averaged target copy is updated by EMA rather than gradient descent. We include the target copy because it occupies the same GPU memory as the

live critic; under a strictly-trainable accounting (target excluded) every SAC row in Table B.2 would shrink by roughly critic, without changing the ordering.

Provenance. Numbers in Table B.2 were not lifted from the corresponding papers (most do not report scalar parameter counts); they were obtained by instantiating each method’s example configuration in code and summing the leaves of the parameter pytree. ARS-paper baselines (SAC-MT, MT-MH-SAC, Soft Modularization, PCGrad-SAC, MOORE, ARS, ARS-LN, ARS-LoRA) come from the official ARS JAX/Flax release [Cho et al., 2025] (<https://github.com/ms-cho/Adaptive-Reward-Scaling-ARS-for-MTRL>); the Meta-World+ MT-family rows (MTMHSAC, PCGrad, Soft Modules, MOORE, PaCo) come from the companion metaworld-algorithms JAX repository [McLean et al., 2025] (<https://github.com/rainx0r/metaworld-algorithms>).

Cross-implementation caveat. Same-named methods can differ between the two source codebases. For example, MOORE is 6,890K (MT10) / 7,403K (MT50) in the ARS reproduction (4 orthogonal 400-wide experts on a SAC-MT backbone) and 6,810K (MT10) / 10,385K (MT50) in the Meta-World+ reproduction (4 experts at MT10, 6 at MT50, plus per-task output heads). We never mix counts across implementations within a single comparison row: Table 2 uses the ARS-paper figures for every V2 baseline (matching the success rates which also come from Tables 1 and 2 of Cho et al. [2025]), and Table D.3 uses the Meta-World+ figures for V1 baselines.

Headline ratios. TOPPO at the headline configuration (LN-c + PopArt on the critic; FG-c on the critic gradient aggregator adds 0 parameters) is 685K (MT10) / 717K (MT50). LN-c (LN affines net of dropped Linear biases on the three hidden layers) and PopArt’s per-task affine (W_i, b_i) together contribute < 1 K parameters at both MT10 and MT50; the no-LN-c, no-PopArt rung (the vanilla MT-PPO entry of the cumulative ladder in Table D.1, i.e., the early-stage rung) is therefore 684K / 716K. Rounded ratios below all use the MT50 headline denominator (717K):

- vs. ARS default (2,597K): we are 27.6% ($1/3.6\times$).
- vs. ARS-LN-1024 (16,267K): we are 4.4% ($1/22.7\times$).
- vs. ARS-LoRA (16,123K): we are 4.4% ($1/22.5\times$).
- vs. PaCo K=20 in Meta-World+ (33,909K): we are 2.1% ($1/47.3\times$).
- vs. MOORE in Meta-World+ (10,385K): we are 6.9% ($1/14.5\times$).

Full table: Table B.2.

Table B.2: Source-counted parameter audit (training-memory totals). TOPPO (685K MT10 / 717K MT50) is $1/3.6\times$ ARS-default, $1/22.7\times$ ARS-LN-1024, and $1/47.3\times$ PaCo K=20 at MT50, supporting the “smaller-and-better” framing. The ARS-paper block [Cho et al., 2025] and Meta-World+ block [McLean et al., 2025] are non-identical reimplementations of same-named methods; counts are never mixed within a comparison row (see Section B.3).

Method (architecture)	Parameters (MT10)	Parameters (MT50)	Notes
Ours: TOPPO [400 × 3]	685K	717K	headline; FG-c aggregator adds 0 params
Ours: Vanilla MT-PPO [400 × 3]	684K	716K	no LN-c, no PopArt (Vanilla MT-PPO rung in Table D.1)
ARS paper: SAC-MT	2,517K	2,597K	actor +2×critic +2×target +α
MT-MH-SAC	2,546K	2,754K	+per-task output head
Soft Modularization	3,454K	3,534K	task-embed + 2 modules × depth 2
PCGrad-SAC	2,517K	2,597K	PCGrad arch-identical to SAC-MT
MOORE	6,890K	7,403K	4 orthogonal 400-wide experts
ARS	2,517K	2,597K	SAC-MT backbone; differs only in loss
ARS-LN (400)	2,530K	2,611K	+LN-c
ARS-LN (1024)	16,062K	16,267K	22.7× our MT50 baseline
ARS-LoRA	3,878K	16,123K	base + LoRA + 2 targets
PaCo / SMT	–	–	not implemented in ARS reference repo
Meta-World+: MTMHSAC / PCGrad	1,759K	2,031K	shared [400]×3 torso, per-task heads
Soft Modules	3,454K	8,030K	(depth, num_modules) = (2,2) MT10 / (4,4) MT50
MOORE	6,810K	10,385K	4 experts MT10 / 6 experts MT50
PaCo (K=5 / K=20)	8,476K	33,909K	compositional Dense; K parameter sets

B.4 PPO-specific adaptations of SAC-based gradient-surgery methods

Provenance. PCGrad, CAGrad, and FairGrad are formulated as generic per-task gradient operators and evaluated primarily on supervised MTL benchmarks (CityScapes / NYUv2 / QM9); their Meta-World evaluations all use SAC (PCGrad / CAGrad on MT10 and MT50; FairGrad on MT10 only) [Yu

et al., 2020a, Liu et al., 2021, Ban and Ji, 2024]. Porting to PPO requires per-task loss decomposition, per-task backward, and a per-side combiner choice (Section 4); the standard PPO machinery (GAE, ratio clip, value clip, Adam, [400×3] MLP) is unchanged, and the four interventions of Section 4 (Table B.1) are the entire delta from vanilla MT-PPO. This subsection documents the few items that are not pinned down by the table or the method section.

Baseline hyperparameters preserved verbatim. We do not re-tune any baseline’s published hyperparameters. CAGrad $c = 0.5$ (MT50) and $c = 0.9$ (MT10) per Liu et al. [2021]; PCGrad has no solver hyperparameters; per-side FairGrad α is in Table B.1.

Solver call frequency. Whereas the SAC originals invoke the solver once per environment step, PPO invokes it once per minibatch inside each rollout’s PPO-epoch loop. Under our schedule (16 PPO repeats per collect × 32 minibatches), that is 512 solver calls per rollout collection on *each* side where a per-task gradient combiner is enabled — the dominant cost driver for any solver scaling worse than $\mathcal{O}(K^3)$ in K , and the practical reason the y -space Newton solver of Algorithm C.2 is non-optional at $K = 50$.

Per-task σ_i rows are decoupled from surgery. The per-task log-stddev $\sigma_i \in \mathbb{R}^{|\mathcal{A}|}$ receives gradient only from task i , so any per-task reweighting acts on row i as a scalar rescale and never aggregates across tasks; only the fully task-shared parameters θ^a, θ^c feed the per-side combiner. The actor/critic partition is exposed to the combiner by a parameter-filter helper that slices the per-task gradient list to each side’s flat slab before invoking it. Code paths for a feature-shared preprocess net (θ_{pre}) and per-task mu/value heads (mu_heads, value_heads) exist but are empty in every reported config.

FairGrad-specific containment. Reference FairGrad does not regularize the Gram matrix and does not clip the output weights w , and we follow that choice. At $\alpha = 1$ the KKT structurally demands large w_i on small-norm rows — $w_i \sim G_{ii}^{-1/2}$ as $\|g_i^c\| \rightarrow 0$ — and clipping w would suppress exactly the rescaling that Theorem 1 and Corollary 1 identify as the mechanism of FG-c. Containment for fp64 safety is therefore split between the solver-internal soft cap $y_{\text{max}} = 50$ and the post-aggregation $\|\cdot\|_2 \leq 1$ clip (both in Table B.1, applied uniformly across all configurations so the comparison isolates the aggregator choice rather than a per-method clip schedule); per-task FG weights and contributions are logged every minibatch so any persistent imbalance is observable online.

B.5 PopArt: implementation note (Welford full-sample statistics)

Our PopArt implementation updates the per-task running statistics (μ_i, σ_i) via Chan–Golub–LeVeque parallel Welford merges [Welford, 1962, Chan et al., 1983] over the full per-task return history. Canonical PopArt [van Hasselt et al., 2016, Eq. 4] presents both options— $\beta_t = 1/t$ recovers the full-history sample mean (mathematically equivalent to our Welford accumulator), while a constant-rate EMA at β is the recommended choice for non-stationary settings; the multi-task PopArt setup of Hessel et al. [2019] adopts the constant- β EMA. Our Welford accumulator therefore matches the $\beta_t = 1/t$ branch of canonical PopArt rather than the constant- β branch typically used in deep RL. After each collect of n_{batch} return targets for task i with batch mean \bar{R}_i and batch sum-of-squared-deviations M_2^{batch} :

$$\begin{aligned} n_{\text{new}} &\leftarrow \text{count}[i] + n_{\text{batch}}, & \delta &\leftarrow \bar{R}_i - \mu_i, \\ \mu_i &\leftarrow \mu_i + \delta \cdot \frac{n_{\text{batch}}}{n_{\text{new}}}, \\ M_2[i] &\leftarrow M_2[i] + M_2^{\text{batch}} + \delta^2 \cdot \frac{\text{count}[i] n_{\text{batch}}}{n_{\text{new}}}, \\ \sigma_i &\leftarrow \max(\sqrt{M_2[i]/n_{\text{new}}}, \sigma_{\text{min}}), & \text{count}[i] &\leftarrow n_{\text{new}}, \end{aligned} \tag{B.1}$$

with $\sigma_{\text{min}} = 10^{-2}$. The PopArt renormalization that adjusts (W_i, b_i) to preserve V_i^{raw} across (μ_i, σ_i) updates runs identically to canonical PopArt and is unaffected by the choice of estimator.

The effective update rate is $n_{\text{batch}}/n_{\text{new}}$, which decays as $\sim 1/n$ and becomes small after many collects. This makes the estimator closer to the marginal return distribution averaged over training than to the return distribution induced by the current policy. Under the non-stationary returns produced by RL training, *the canonical EMA at a tuned β is likely the better estimator.*

Effect on the paper’s claims. Theorem 1 and Corollary 1 hold for any positive task-wise rescaling $\mathbf{c} \in \mathbb{R}_{>0}^K$, so FG-c absorbs Welford-PopArt’s and EMA-PopArt’s $c_i = \sigma_i^{-2}$ identically; the empirical numbers in Tables 2 and D.1 are about our Welford variant and we do not claim them as canonical-EMA-PopArt reproductions. The two estimators are closest precisely during the early-training phase that determines whether the self-reinforcing tail trap (Section 3) is set or escaped: with $\text{count}[i]$ small, Welford’s effective update rate $n_{\text{batch}}/n_{\text{new}}$ is close to 1, and a canonical EMA at small β has not yet accumulated enough history for its geometric tail to dominate, so both σ_i values are driven by the most recent batches. The two diverge only in mid-to-late training, where Welford freezes near the marginal-return distribution (rate $\sim 1/n$) while EMA keeps tracking the current policy’s distribution at constant β ; by that point the tail tasks have either been recovered or locked in, bounding the estimator choice’s effect on final-outcome metrics. The same argument applies under V1’s heterogeneous reward scales, supporting our interpretation (Section D.5) that the V1 Corollary 1 inversion is driven primarily by PopArt’s non-rescaling channels rather than by the Welford-vs-EMA gap.

C Theoretical Details

C.1 TOPPO pseudocode

Algorithm C.1 expands the compact Algorithm 1 (Section 4) with the bookkeeping that the main-text version folds into surrounding loop headers, mirroring the released implementation. The differences from vanilla MT-PPO are localized to four points: PopArt update before the minibatch loop (line 3), task-stratified minibatching (line 6), per-task loss decomposition with one backward per task (lines 9–12), and the per-side gradient combiners FG-c / PCGrad-a (lines 13–14). PPO’s GAE, ratio clip, value clip, recompute-advantage, post-aggregation gradient-norm clip, and Adam step are unchanged.

Algorithm C.1 TOPPO: a PPO collect-and-update phase.

Require: Tasks $\{\mathcal{M}_i\}_{i=1}^K$, shared params $\theta = (\theta^a, \theta^c)$ with **[LN-c]** on critic hidden layers and per-task PopArt affine $\{(\sigma_i, \mu_i)\}$, repeats R , minibatch size b , clip ϵ , max gradient norm τ

- 1: Rollout $\mathcal{B} = \bigcup_i \mathcal{B}_i$ under $\pi_{\theta_{\text{old}}^a}$ (uniform per task); calculate per-task GAE $\hat{A}_t^{(i)}$ and value targets $\hat{V}_t^{(i), \text{targ}}$ on raw returns
 - 2: **[PopArt]** update (μ_i, σ_i) via Welford on $\{\hat{V}_t^{(i), \text{targ}}\}$ (Eq. (B.1)) and PopArt-renormalize the per-task affine head so raw V is preserved (Section 4.1)
 - 3: **for** $r = 1$ **to** R **do**
 - 4: **if** $r > 1$ **then**
 - 5: recompute $\hat{A}_t^{(i)}, \hat{V}_t^{(i), \text{targ}}$ on \mathcal{B} under current V_{θ^c}
 - 6: **end if**
 - 7: **for** each task-stratified minibatch $\mathcal{B}^{\text{mb}} \subset \mathcal{B}$ of size b **do**
 - 8: normalize advantages within each task slice of \mathcal{B}^{mb} ; map critic targets to PopArt space $(\hat{V}_t^{(i), \text{targ}} - \mu_i)/\sigma_i$ as in Section 4.1
 - 9: **for** $i = 1$ **to** K such that $\mathcal{B}_i^{\text{mb}} \neq \emptyset$ **do**
 - 10: $L_i \leftarrow L_i^a(\theta^a) + c_w L_i^{c, \text{PopArt}}(\theta^c) - c_e H_i(\theta^a)$ on $\mathcal{B}_i^{\text{mb}}$ (Eq. (1))
 - 11: backward $\mathbf{g}_i \leftarrow \nabla_{\theta} L_i$ and cache flat actor and PopArt critic slabs $(\mathbf{g}_i^a, \mathbf{g}_i^{c, \text{PopArt}})$
 - 12: **end for**
 - 13: **[FG-c ($\alpha=1$)]** solve $\mathbf{G}^c \mathbf{w} = \mathbf{w}^{-1}$ via Algorithm C.2, then $\mathbf{d}^c \leftarrow \sum_i w_i \mathbf{g}_i^{c, \text{PopArt}}$ (Section 4.3)
 - 14: **[PCGrad-a]** $\mathbf{d}^a \leftarrow \text{PCGrad}(\mathbf{g}_1^a, \dots, \mathbf{g}_K^a)$ actor-side surgery
 - 15: rescale $(\mathbf{d}^a, \mathbf{d}^c)$ by $\min(1, \tau/\|(\mathbf{d}^a, \mathbf{d}^c)\|_2)$; Adam step on θ
 - 16: **end for**
 - 17: **end for**
-

C.2 α -fairness family and KKT derivation

This appendix expands Section 4.3 with three pieces deferred from the main text: (i) the interpretation of U_α in Eq. (3) as a one-parameter fairness family, (ii) the precise meaning of “per-task contribution

x_i ” in Eq. (C.1) and the canonical scaling that pins down \mathbf{w} in the FairGrad program, and (iii) the derivation, via a strictly convex unconstrained program, of the KKT condition $\mathbf{G}^c \mathbf{w} = \mathbf{w}^{-1/\alpha}$ stated in Section 4.3.

Family interpretation. U_α [Mo and Walrand, 2000, Kelly, 1997] is strictly concave on $\mathbb{R}_{>0}$ for every $\alpha > 0$, and as α varies over $(0, \infty)$ it interpolates classical social-welfare rules: utilitarian sum as $\alpha \rightarrow 0^+$ (each unit of x_i has equal marginal value), Nash bargaining at $\alpha = 1$ [Nash, 1950] (the log-utility / geometric-mean solution), and Rawlsian max-min as $\alpha \rightarrow \infty$ (the smallest x_i dominates). Larger α thus up-weights small-share agents — equivalently, in our setting, gives more aggregator budget to tasks whose contribution to the combined critic gradient is currently small.

Per-task contribution and the canonical scaling. Write $\mathbf{d} := \sum_i w_i \mathbf{g}_i^c$ for the combined critic gradient. “Per-task contribution” refers to the inner product

$$x_i := \mathbf{g}_i^c \top \mathbf{d} = (\mathbf{G}^c \mathbf{w})_i, \quad (\text{C.1})$$

i.e. how much task i ’s gradient agrees with the combined direction; $x_i > 0$ is the linearized loss decrease task i obtains under a unit step along \mathbf{d} . The bare welfare $\sum_i U_\alpha((\mathbf{G}^c \mathbf{w})_i)$ has no interior maximizer along positive rays $\mathbf{w} \mapsto t\mathbf{w}$ (for $0 < \alpha \leq 1$ it grows without bound as $t \rightarrow \infty$; for $\alpha > 1$ it approaches its supremum 0 only in that limit), so a normalization is needed to pin down a canonical \mathbf{w} . Geometrically, $\mathbf{w}^\top \mathbf{G}^c \mathbf{w} = \|\mathbf{d}\|^2$, so any normalization of \mathbf{w} corresponds to a choice of $\|\mathbf{d}\|$. Throughout the paper we adopt the *canonical scaling* that yields the dimensionless KKT $\mathbf{G}^c \mathbf{w} = \mathbf{w}^{-1/\alpha}$ used in Section 4.3, Theorem 1, and Corollary 1; for $\alpha = 1$, this canonical \mathbf{w} satisfies $\|\mathbf{d}\|^2 = \mathbf{w}^\top \mathbf{G}^c \mathbf{w} = K$ rather than 1 (Theorem 1).

Derivation of the FairGrad KKT condition. For $\alpha = 1$ (the case used throughout the paper), the canonical-scaling solution is the unique minimizer of the strictly convex unconstrained program

$$\min_{\mathbf{w} \in \mathbb{R}_{>0}^K} \Phi_1(\mathbf{w}) := \frac{1}{2} \mathbf{w}^\top \mathbf{G}^c \mathbf{w} - \sum_{i=1}^K \log w_i. \quad (\text{C.2})$$

Strict convexity follows from $\nabla^2 \Phi_1(\mathbf{w}) = \mathbf{G}^c + \text{diag}(w_i^{-2}) \succ 0$ on $\mathbb{R}_{>0}^K$ (since $\mathbf{G}^c \succ 0$ by the linear-independence assumption); existence and uniqueness then follow because $\Phi_1(\mathbf{w}) \rightarrow +\infty$ both on $\partial \mathbb{R}_{>0}^K$ (via $-\sum_i \log w_i \rightarrow +\infty$ as any $w_i \rightarrow 0^+$) and as $\|\mathbf{w}\| \rightarrow \infty$ (via $\mathbf{w}^\top \mathbf{G}^c \mathbf{w} \geq \lambda_{\min}(\mathbf{G}^c) \|\mathbf{w}\|^2$). Stationarity $\nabla \Phi_1(\mathbf{w}^*) = \mathbf{0}$ reads $\mathbf{G}^c \mathbf{w}^* - (\mathbf{w}^*)^{-1} = \mathbf{0}$, i.e. the dimensionless KKT

$$\mathbf{G}^c \mathbf{w}^* = (\mathbf{w}^*)^{-1} \quad (\text{componentwise}),$$

stated in Section 4.3, on which Theorem 1 and Corollary 1 build. This canonical solution coincides with the constrained α -fairness program $\max \sum_i \log((\mathbf{G}^c \mathbf{w})_i)$ subject to $\mathbf{w}^\top \mathbf{G}^c \mathbf{w} = K$: the constraint value K is precisely what makes the Lagrange multiplier equal 1 at the optimum, eliminating the rescaling step needed under the conventional unit-norm normalization $\mathbf{w}^\top \mathbf{G}^c \mathbf{w} = 1$. The unconstrained form Eq. (C.2) avoids carrying a Lagrange multiplier through the derivation. For general $\alpha > 0$, the same construction with $\sum_i \log w_i$ replaced by $\frac{\alpha}{\alpha-1} \sum_i w_i^{1-1/\alpha}$ ($\alpha \neq 1$) gives the KKT $\mathbf{G}^c \mathbf{w} = \mathbf{w}^{-1/\alpha}$ via the same stationarity calculation; the boundary argument is replaced by gradient blow-up $\partial \Phi_\alpha / \partial w_i = (\mathbf{G}^c \mathbf{w})_i - w_i^{-1/\alpha} \rightarrow -\infty$ as $w_i \rightarrow 0^+$, which still forces an interior minimizer. The KKT couples per-task scale (diagonal \mathbf{G}_{ii}^c , how loud each task is on its own) with direction conflict (off-diagonals, how compatibly two tasks pull).

C.3 Aggregator family taxonomy and cone containment

Theorem C.1 (Shared cone containment). *Let $\text{cone}^+ \{\mathbf{g}_1, \dots, \mathbf{g}_K\} := \{\sum_i w_i \mathbf{g}_i : w_i \geq 0\}$ denote the closed conic hull (non-negative combinations) of the per-task gradient set. The combined gradient produced by FairGrad (any $\alpha > 0$), PCGrad [Yu et al., 2020a], CAGrad [Liu et al., 2021], FAMO [Liu et al., 2023], DWA [Liu et al., 2019], and uncertainty weighting [Kendall et al., 2018] lies in $\text{cone}^+ \{\mathbf{g}_1, \dots, \mathbf{g}_K\}$.*

Proof. For FairGrad/FAMO/DWA/UW, the combined gradient is $\sum_i w_i \mathbf{g}_i$ with $w_i \geq 0$ by construction (FairGrad’s KKT solves on $\mathbb{R}_{>0}^K$ for $\alpha > 0$; FAMO/DWA/UW use loss-level reweighting

with non-negative weights, so $\nabla \sum_i w_i L_i = \sum_i w_i \mathbf{g}_i$. For CAGrad, the combined gradient is $\sum_i (\frac{1}{K} + w_i^* \lambda^*) \mathbf{g}_i$ with $w_i^* \geq 0$ on the simplex and $\lambda^* \geq 0$ [Liu et al., 2021], so the coefficient on each \mathbf{g}_i is $\geq \frac{1}{K} > 0$. For PCGrad, induct over the projection schedule. Let $S_{<k}$ denote the (ordered) set of tasks already projected against in task i 's inner loop before step k . Base case ($k = 0$): $\mathbf{g}'_i = \mathbf{g}_i$, with coefficient 1 on \mathbf{g}_i and $\mu_{i,m} = 0$ for all $m \neq i$. Inductive step: at step k with $\mathbf{g}'_i = \mathbf{g}_i + \sum_{m \in S_{<k}} \mu_{i,m} \mathbf{g}_m$ ($\mu_{i,m} \geq 0$), the projection is taken against the *original* \mathbf{g}_{j_k} (Yu et al., 2020a, Algorithm 1); If $\langle \mathbf{g}'_i, \mathbf{g}_{j_k} \rangle \geq 0$ no update; else the update adds $-\langle \mathbf{g}'_i, \mathbf{g}_{j_k} \rangle / \|\mathbf{g}_{j_k}\|^2 > 0$ to the (non-negative) coefficient on \mathbf{g}_{j_k} . Invariant preserved; final \mathbf{g}_i^{PC} is a non-negative combination of $\{\mathbf{g}_1, \dots, \mathbf{g}_K\}$. The combined gradient $\mathbf{g}^{\text{PC}} = \frac{1}{K} \sum_i \mathbf{g}_i^{\text{PC}}$ is then a non-negative combination of the same set, hence in $\text{cone}^+ \{\mathbf{g}_1, \dots, \mathbf{g}_K\}$. \square

Remark C.1 (FG at $\alpha=1$ recovers Nash-MTL). At $\alpha=1$, the α -fairness utility is $U_1(x) = \sum_i \log x_i$, the Nash welfare [Nash, 1950, Kelly, 1997, Mo and Walrand, 2000]. Applied to per-task improvement $u_i = \mathbf{g}_i^\top \mathbf{d}$ along a feasible descent direction $\mathbf{d} \in \text{cone}^+ \{\mathbf{g}_1, \dots, \mathbf{g}_K\}$, the FG $\alpha=1$ program reduces to $\mathbf{d}^* = \arg \max_{\mathbf{d} \in \text{cone}^+ \{\mathbf{g}_i\}} \sum_i \log(\mathbf{g}_i^\top \mathbf{d})$, which is the Nash bargaining problem solved by Nash-MTL [Navon et al., 2022]. Both methods share the same per-component KKT $w_i(\mathbf{G}\mathbf{w})_i = 1$ (the precursor to the \sqrt{K} -energy identity of Theorem 1); they differ only in solver (CCP-via-CVXPY for Nash-MTL vs. scipy least-squares for the original FairGrad vs. our y -space Newton).

Implication. Theorem C.1 reframes the gradient-aggregation design space: methods differ in which point inside the same shared cone they select, not in the cone itself. FAMO/DWA/UW pick a Gram-blind point; PCGrad picks a point determined by $\text{sign}(\mathbf{G}_{ij})$ via random-order projection; CAGrad picks the solution of a constrained QP on \mathbf{G} ; FairGrad picks the α -fairness KKT solution on the full Gram. Among these, only $\alpha=1$ FG carries the closed-form \sqrt{K} -energy identity and scale-invariance of Theorem 1.

C.4 Proof of Theorem 1 (scale invariance)

We write \mathbf{w}^* for the theorem's \mathbf{w} throughout, reserving \mathbf{w} as the optimization variable. Thus $\mathbf{w}^* \in \mathbb{R}_{>0}^K$ denotes the unique positive solution of the $\alpha = 1$ KKT $\mathbf{G}\mathbf{w} = \mathbf{w}^{-1}$. Fix any $\mathbf{c} \in \mathbb{R}_{>0}^K$, set $\tilde{\mathbf{g}}_i := c_i \mathbf{g}_i$ and $D := \text{diag}(\mathbf{c})$, and write $\tilde{\mathbf{G}} := D\mathbf{G}D$ for the rescaled Gram. We proceed in four steps.

Step 1 (existence and uniqueness). The KKT $\mathbf{G}\mathbf{w} = \mathbf{w}^{-1}$ is the $\alpha = 1$ specialization of the strictly convex unconstrained program (C.2), which admits a unique positive minimizer by the argument given there. Since D is invertible and $\mathbf{G} \succ 0$, congruence yields $\tilde{\mathbf{G}} = D\mathbf{G}D \succ 0$; applying the same argument to (C.2) with \mathbf{G} replaced by $\tilde{\mathbf{G}}$ gives a unique positive solution of the rescaled KKT $\tilde{\mathbf{G}}\tilde{\mathbf{w}} = \tilde{\mathbf{w}}^{-1}$.

Step 2 (norm identity $\|\sum_i w_i^ \mathbf{g}_i\|^2 = K$).* Componentwise, $(\mathbf{G}\mathbf{w}^*)_i = 1/w_i^*$, hence $w_i^*(\mathbf{G}\mathbf{w}^*)_i = 1$ for every i . Summing,

$$(\mathbf{w}^*)^\top \mathbf{G}\mathbf{w}^* = \sum_{i=1}^K w_i^*(\mathbf{G}\mathbf{w}^*)_i = K.$$

Expanding the quadratic form via $\mathbf{G}_{ij} = \langle \mathbf{g}_i, \mathbf{g}_j \rangle$ gives

$$\left\| \sum_i w_i^* \mathbf{g}_i \right\|^2 = \sum_{i,j} w_i^* w_j^* \langle \mathbf{g}_i, \mathbf{g}_j \rangle = (\mathbf{w}^*)^\top \mathbf{G}\mathbf{w}^* = K.$$

Step 3 (scale invariance at $\alpha = 1$). Define $\tilde{\mathbf{w}} := \mathbf{w}^* \circ \mathbf{c}$, i.e. $\tilde{w}_i = w_i^*/c_i$. We verify that $\tilde{\mathbf{w}}$ solves the rescaled KKT and preserves the combined update.

(3a) Rescaled KKT. Using $\tilde{\mathbf{G}}_{ij} = c_i c_j \mathbf{G}_{ij}$ and $c_j \tilde{w}_j = w_j^*$,

$$(\tilde{\mathbf{G}}\tilde{\mathbf{w}})_i = c_i \sum_j \mathbf{G}_{ij} (c_j \tilde{w}_j) = c_i \sum_j \mathbf{G}_{ij} w_j^* = c_i (\mathbf{G}\mathbf{w}^*)_i = \frac{c_i}{w_i^*} = \frac{1}{\tilde{w}_i}.$$

Hence $\tilde{\mathbf{G}}\tilde{\mathbf{w}} = \tilde{\mathbf{w}}^{-1}$, and by Step 1's uniqueness $\tilde{\mathbf{w}}$ is the rescaled FairGrad output.

(3b) Combined-update preservation. Direct substitution gives

$$\sum_i \tilde{w}_i \tilde{\mathbf{g}}_i = \sum_i \frac{w_i^*}{c_i} (c_i \mathbf{g}_i) = \sum_i w_i^* \mathbf{g}_i.$$

(In fact, combined-update preservation already pins down $\tilde{\mathbf{w}}$: any $\tilde{\mathbf{w}} \in \mathbb{R}_{>0}^K$ with $\sum_i \tilde{w}_i \tilde{\mathbf{g}}_i = \sum_i w_i^* \mathbf{g}_i$ satisfies $\sum_i (c_i \tilde{w}_i - w_i^*) \mathbf{g}_i = 0$, and linear independence of $\{\mathbf{g}_i\}$ forces $\tilde{w}_i = w_i^*/c_i$.)

Step 4 (necessity of $\alpha = 1$). Fix $0 < \alpha \neq 1$ and suppose, for contradiction, that the FairGrad output is invariant under all positive task-wise rescalings. The combined-update preservation argument in Step 3b uses only linear independence and is independent of α , so by hypothesis the rescaled solution must again be $\tilde{w}_i = w_i^*/c_i$, where now \mathbf{w}^* solves the original α -fairness KKT $(\mathbf{G}\mathbf{w}^*)_i = (w_i^*)^{-1/\alpha}$. The same factoring as in Step 3a then yields

$$(\tilde{\mathbf{G}}\tilde{\mathbf{w}})_i = c_i (\mathbf{G}\mathbf{w}^*)_i = c_i (w_i^*)^{-1/\alpha} = c_i (c_i \tilde{w}_i)^{-1/\alpha} = c_i^{1-1/\alpha} \tilde{w}_i^{-1/\alpha}.$$

The rescaled α -fairness KKT requires the right-hand side to equal $\tilde{w}_i^{-1/\alpha}$, so $c_i^{1-1/\alpha} = 1$ must hold for every $c \in \mathbb{R}_{>0}^K$, which forces $1 - 1/\alpha = 0$, i.e. $\alpha = 1$. Hence $\alpha = 1$ is the unique exponent in the family for which the FairGrad output is invariant under arbitrary positive task-wise rescalings.

C.5 y -Newton solver derivation and benchmark protocol

This appendix expands Section 4 with derivations.

Setup and Newton step derivation. Reparametrize $\mathbf{w} = e^{\mathbf{w}_y}$ (positivity automatic; search variable on \mathbb{R}^K). The shipped solver writes the Armijo test on the residual norm itself rather than the squared norm; both are equivalent up to a $\sqrt{1-c_1 t}$ vs. $1-c_1 t$ factor (the unsquared form is slightly more aggressive). Tier-1 declares convergence when $\|F(\mathbf{w}_y)\|$ drops below $\eta = 10^{-2}$; the source also exposes a tighter parameter $\tau = 10^{-8}$ for theorem-verification calls (Section 4, \sqrt{K} -energy reproducibility), but in the production solve path with $\eta = 10^{-2}$ the $r \leq \tau$ branch is mathematically redundant and never independently triggers. The y -space residual and Jacobian are

$$F(\mathbf{w}_y) = \mathbf{G}^c \exp(\mathbf{w}_y) - \exp(-\mathbf{w}_y/\alpha), \quad (\text{C.3})$$

$$J(\mathbf{w}_y) = \mathbf{G}^c \text{diag}(\exp(\mathbf{w}_y)) + \frac{1}{\alpha} \text{diag}(\exp(-\mathbf{w}_y/\alpha)). \quad (\text{C.4})$$

The componentwise derivative

$$\frac{\partial F_i}{\partial w_{y,j}} = \mathbf{G}_{ij}^c \exp(w_{y,j}) + \frac{1}{\alpha} \delta_{ij} \exp(-w_{y,i}/\alpha), \quad (\text{C.5})$$

assembles to (C.4); in code, J is built by broadcasting $\exp(\mathbf{w}_y)$ along the columns of \mathbf{G}^c plus a diagonal increment, avoiding explicit `diag` materialization. The full procedure — diagonal warm-start, damped y -Newton with Armijo line search, and the two fallback tiers — is given in Algorithm C.2.

Closed-form warm-start (uniqueness).

Proposition C.1 (Diagonal closed form). *If \mathbf{G}^c is diagonal with strictly positive entries, the unique positive solution of the FG-KKT is $w_i^{\text{diag}} = G_{ii}^{-\alpha/(\alpha+1)}$.*

Proof. Diagonal \mathbf{G}^c decouples the KKT into $G_{ii} w_i = w_i^{-1/\alpha}$. Multiply by $w_i^{1/\alpha}$: $G_{ii} w_i^{1+1/\alpha} = 1$, so $w_i = G_{ii}^{-\alpha/(\alpha+1)}$. The map $w \mapsto G_{ii} w - w^{-1/\alpha}$ is strictly increasing on $\mathbb{R}_{>0}$ (derivative $G_{ii} + (1/\alpha)w^{-1-1/\alpha} > 0$) — solution unique. \square

Why the warm-start matters.

- For non-diagonal \mathbf{G}^c : Proposition C.1 is exact under the diagonal-Gram approximation; mid-training PPO Gram is diagonal-dominant ($\mathbf{G}_{ii}^c \gg \sum_{j \neq i} |\mathbf{G}_{ij}^c|$ for active tasks), so w^{diag} converges within 2 Newton iterations on every regime in Table C.1 except the $K=50$ rand-struct stress test (row 3, where adversarial cross-coupling stalls the warm-start at the 50-iter cap; see also row 3 caveat in Table C.1).

Algorithm C.2 y -space projected damped Newton solver for the FG-KKT $\mathbf{G}^c \mathbf{w} = \mathbf{w}^{-1/\alpha}$, with three-tier fallback. Called once per PPO minibatch (Section B.4).

Require: Critic Gram $\mathbf{G}^c \in \mathbb{R}_{>0}^{K \times K}$ (fp64), exponent $\alpha > 0$, residual target $\eta = 10^{-2}$, soft cap $y_{\max} = 50$, max outer iters $N = 50$, max Armijo backtracks $B = 30$, Armijo $c_1 = 10^{-4}$

Ensure: Weights $\mathbf{w} \in \mathbb{R}_{>0}^K$ with $\|F(\mathbf{w}_y)\| \leq \eta$ when convergent

- 1: $\mathbf{w}_y \leftarrow -\frac{\alpha}{\alpha+1} \log \max(\text{diag}(\mathbf{G}^c), \varepsilon)$ {diagonal warm-start (Proposition C.1); ε guards log 0}
- 2: $\mathbf{w}_y \leftarrow \text{clip}(\mathbf{w}_y, -y_{\max}, y_{\max})$ {soft cap}
- 3: **for** $k = 1$ **to** N **do**
- 4: $F \leftarrow \mathbf{G}^c \exp(\mathbf{w}_y) - \exp(-\mathbf{w}_y/\alpha)$ {eq. (C.3)}
- 5: **if** $\|F\| \leq \eta$ **then**
- 6: **return** $\exp(\mathbf{w}_y)$
- 7: **end if**
- 8: $J \leftarrow \mathbf{G}^c \cdot \text{diag}(\exp(\mathbf{w}_y)) + \frac{1}{\alpha} \text{diag}(\exp(-\mathbf{w}_y/\alpha))$ {eq. (C.4)}
- 9: solve $J \mathbf{d} = -F$ in fp64
- 10: $t \leftarrow 1$; *accepted* \leftarrow false
- 11: **for** $j = 1$ **to** B **do**
- 12: $\mathbf{w}_y^{\text{trial}} \leftarrow \min(\mathbf{w}_y + t \mathbf{d}, y_{\max})$
- 13: $F^{\text{trial}} \leftarrow \mathbf{G}^c \exp(\mathbf{w}_y^{\text{trial}}) - \exp(-\mathbf{w}_y^{\text{trial}}/\alpha)$
- 14: **if** $\|F^{\text{trial}}\| < (1 - c_1 t) \|F\|$ **then**
- 15: $\mathbf{w}_y \leftarrow \mathbf{w}_y^{\text{trial}}$; *accepted* \leftarrow true; **break out of inner loop**
- 16: **end if**
- 17: $t \leftarrow t/2$
- 18: **end for**
- 19: **if not accepted then**
- 20: **break out of outer loop** {Armijo exhausted; pass current \mathbf{w}_y to Tier 2}
- 21: **end if**
- 22: **end for**
- 23: *Tier 2: Newton did not reach $\eta \rightarrow$ scipy least-squares warm-started from $\exp(\mathbf{w}_y)$*
- 24: $\mathbf{w} \leftarrow \text{scipy.optimize.least_squares}(F, x_0 = \max(\exp(\mathbf{w}_y), \varepsilon), \text{bounds} = (\varepsilon, \infty))$
- 25: **if** *res.success* and \mathbf{w} is finite **then**
- 26: **return** \mathbf{w}
- 27: **end if**
- 28: *Tier 3: scipy also failed \rightarrow uniform fallback, flag failure to online diagnostics*
- 29: **return** $\mathbf{1}_K/K$

- Dead-task rows ($\mathbf{G}_{ii}^c \rightarrow 0$): warm-start $\rightarrow \infty$ in the correct direction; uniform cold-start $w_y \equiv -\log K$ cannot reproduce this.
- On Gram with ≥ 2 simultaneously small-norm rows: Newton’s last iterate is up to 40 log-units closer to the truth in y -space than scipy’s $1/K$ default (i.e. $\sim e^{40} \approx 2 \times 10^{17} \times$ closer in w -space), which both improves Tier-2 success probability and shortens Tier-2 wall clock when it does fire. The diagnostics in Section B.4 log used_scipy_fallback and solver_fallback per minibatch so Tier-2 / Tier-3 firing rates are observable in the sweep.

Newton step in the small-norm regime.

- Row i with $\mathbf{G}_{i,:}^c \rightarrow 0$: $F_i \rightarrow -\exp(-w_{y,i}/\alpha)$, $J_{ii} \rightarrow (1/\alpha) \exp(-w_{y,i}/\alpha)$.
- Newton step: $\Delta w_{y,i} = -F_i/J_{ii} \rightarrow \alpha$ — exactly α in the row-deficient limit $\mathbf{G}_{i,:}^c \rightarrow 0$.
- Iter count for cold-start ($w_y \equiv -\log K$) to climb to the true small-norm-task weight at $y_i^* \approx 50$: $\lceil (y^* + \log K)/\alpha \rceil \approx 54$ at $\alpha = 1$ (the slowest setting in our matrix), exceeding the $N = 50$ outer cap. Cold-start nevertheless terminates the $r \leq \eta$ check at ~ 10 outer iterations on rows 3–5 of Table C.1 (e.g. row 4: $r_{\text{cold}} = 6.2 \cdot 10^{-3} < \eta$), but at that point its small-norm weight is stalled near $w_i \sim e^{10}$ rather than the warm-start’s $\sim e^{50}$ — KKT-residual-converged yet tens of log-units off in the small-norm coordinate. The warm-start of Proposition C.1 skips this stall by initializing each w_i at its diagonal-Gram closed form.
- Structural origin of the ~ 50 – $1,450 \times$ speedup vs. scipy across realistic Gram regimes (Table C.1). The absolute upper end ($1,442 \times$, row 2: heterogeneous $K=10$) and the production-realistic upper

end (1,344×, row 4: $K=50$ \perp -active single small-norm row) are within $\sim 7\%$ of each other; the lower end (48×, row 1) is the well-conditioned baseline where scipy’s TRF still benefits from a forward-Jacobian fast path.

fp64 throughout.

- Gram computation, residual, line search, final per-task contribution sum: all fp64.
- Dead-task: $\|\mathbf{g}_i^c\|^2$ in fp32 can underflow (10^{-22} grad $\rightarrow 10^{-44}$, below fp32 smallest normal). fp64 retains ~ 308 -decimal-digit dynamic range — distinguishes “literally zero” from “very small but informative”.
- Soft cap $w_y \leq y_{\max} = 50$ keeps $w \leq e^{50} \approx 5 \times 10^{21}$ — fp64-safe.
- Combine step $\sum_i w_i \mathbf{g}_i^c$ also fp64: intermediate products at $w_i \sim 10^{22}$ can transiently overflow fp32 even when final sum is bounded.

Wall-clock benchmark protocol.

- Synthetic Gaussian per-task gradients $\mathbf{g}_i \in \mathbb{R}^D$ with $D = 1024$ and $\alpha = 1$ (matching the per-side default of Section 4); Gram $\mathbf{G}^c = [\mathbf{g}_i^\top \mathbf{g}_j]_{i,j}$ assembled in fp64.
- Five regimes spanning the (per-task norm spread, off-diagonal structure) plane: well-conditioned $K=50$ at spread $1\times$; heterogeneous $K=10$ with random-direction small-norm rows at $10^6\times$ spread; and three high-spread $K=50$ regimes at $10^8\times$ spread distinguished by structure — random Gaussian (rand, synthetic stress test), orthogonal-to-active single small-norm row (\perp , the actual Meta-World PPO geometry under PopArt-rescale events), and orthogonal-to-active 25% small-norm rows (\perp 25%, production worst case).
- Four solvers per regime: scipy least_squares (verbatim FairGrad-paper reference, bounds=(0, ∞), no $\max(x, \epsilon)$ clip), SGD+momentum (verbatim FairGrad-RL release, lr=0.1, momentum=0.5, niter=20, track-best), y -Newton with uniform cold start, and y -Newton with the diagonal warm-start of Proposition C.1 (our production solver).
- Each (solver \times regime) cell timed $7\times$ with warm timing (first run discarded); we report the median.
- Speedup = ratio scipy/Newton-warm in median per-call wall clock, with active-task contributions matched within 1%.
- Numbers in Table C.1. A separate production-measured benchmark on real MT10/MT50 PPO Gram captured during training reproduces the same warm-vs-scipy ordering at $1.5\text{--}3\times$ faster scipy absolute times.

Table C.1: **FairGrad solver benchmark against verbatim upstream baselines.** Median wall time per solve (ms) and KKT residual $\|\mathbf{G}^c \mathbf{w} - \mathbf{w}^{-1/\alpha}\|$ at termination across the five Gram regimes of Section C.5, with convergence target $\eta = 10^{-2}$. The \times marker flags that the FG-RL SGD solver exhausts its upstream-fixed niter=20 budget without reaching η on every regime; the Speedup column reports y -Newton-warm vs. scipy. Row 3 is the rand-struct $K=50$ stress test where warm-start cross-coupling stalls above η , so its $95\times$ entry is parenthetical; on row 5, warm y -Newton’s residual $4.7 \cdot 10^{-5}$ undercuts scipy’s $5.3 \cdot 10^{-3}$ plateau.

Regime	Wall time per solve (ms)				KKT residual at termination				Speedup
	scipy (FG paper)	SGD (FG-RL)	y-N (cold)	y-N (warm)	scipy (FG paper)	SGD (FG-RL)	y-N (cold)	y-N (warm)	
$K=50$, spread $1\times$	14.5	10.6 \times	0.43	0.30	$1.8 \cdot 10^{-13}$	$5.0 \cdot 10^1$	$3.4 \cdot 10^{-7}$	$2.4 \cdot 10^{-5}$	48 \times
$K=10$, rand, spread 10^6	195	9.0 \times	0.64	0.14	$7.7 \cdot 10^{-10}$	$5.2 \cdot 10^6$	$2.7 \cdot 10^{-9}$	$4.8 \cdot 10^{-5}$	1,442 \times
$K=50$, rand, spread 10^8 (stress test)	733	10.1 \times	0.84	7.7	$5.6 \cdot 10^{-7}$	$5.6 \cdot 10^1$	$6.2 \cdot 10^{-3}$	$2.0 \cdot 10^{-2}$ (rand stall)	95 \times (rand-stall)
$K=50$, \perp , spread 10^8 (production)	288	10.2 \times	0.84	0.22	$9.3 \cdot 10^{-11}$	$5.6 \cdot 10^1$	$6.2 \cdot 10^{-3}$	$3.2 \cdot 10^{-5}$	1,344 \times
$K=50$, \perp 25%, spread 10^8	27.4	10.2 \times	0.93	0.21	$5.3 \cdot 10^{-3}$	$7.8 \cdot 10^1$	$7.9 \cdot 10^{-3}$	4.7 $\cdot 10^{-5}$	131 \times

D Additional Experimental Results

D.1 Detailed ablation results

This appendix expands the main-text ablation summary (Section 5.3) with the underlying tables and per-cell analysis.

Critic-side intervention cube (V2). Table D.1 reports the 2×2 PopArt \times FG-c sub-cube of the intervention cube (LN-c on, actor=default); the full 5-rung cumulative ladder and per-axis mechanism

mapping are in Table 2 and Figure 4 and Section 5.3. Two scope caveats matter for reading the table: the predicted PopArt-marginal collapse signature is at training-outcome scale, not a direct verification of the per-minibatch identity, and the table does not show that every non-aggregation channel of PopArt has zero effect. The synthetic per-minibatch verification of Theorem 1 is in Figure D.5 (Section D.3); the training-time analog at the aggregator-output level is the (c) \equiv (d) coincidence in Figure D.4. The complementary regime where PopArt’s non-rescaling channels become load-bearing is the V1 sweep below.

Table D.1: **PopArt \times $\alpha=1$ FG-c interaction on MT50.** The 2×2 sub-cube isolates whether adding FG-c absorbs PopArt’s worst-10 marginal at training-outcome scale, the signature predicted by Corollary 1; the deltas below the table confirm collapse from rows 1 \rightarrow 2 to rows 3 \rightarrow 4. All rows use actor=default with LN-c on; 10 seeds, final checkpoint, 100M env steps.

Configuration	PopArt	FG-c	MT50 mean	MT50 worst-10
+LN-c (base)	–	–	87.5 \pm 2.4	42.3 \pm 10.1
+LN-c +PopArt	✓	–	88.9 \pm 2.3	48.9 \pm 9.0
+LN-c +FG-c	–	✓	89.7 \pm 1.6	52.6 \pm 7.6
+LN-c +PopArt +FG-c	✓	✓	90.1 \pm 2.3	52.4 \pm 11.3

Δ_{PopArt} without FG-c (rows 1 \rightarrow 2): 1.36% \uparrow mean, **6.64%** \uparrow worst-10. Δ_{PopArt} with FG-c (rows 3 \rightarrow 4): 0.39% \uparrow mean, **0.22%** \downarrow worst-10.

LayerNorm placement ablation. On MT10 with PopArt held fixed (default actor and critic combiners, 10 seeds), symmetric LN on both actor and critic reaches $93.06 \pm 4.61\%$ final mean vs. $96.76 \pm 1.52\%$ for critic-only LN — a 3.70% \downarrow mean drop with $\sim 3\times$ wider seed std. We attribute this tentatively to PPO’s clipped policy ratio: LN on actor pre-activations changes the mapping from hidden features to the action-mean projection across minibatch updates, which can inflate $|\log \pi(a|s)/\pi_{\text{old}}(a|s)|$ and trigger the ratio clip more frequently; the critic has no analogous ratio constraint and is unaffected by LN-c. Given the MT10 result we did not extend symmetric LN to a 10-seed MT50 sweep.

Per-side combiner asymmetry. Table D.2 reports the per-side cube. PCGrad-a’s contribution is concentrated on the tail tasks: switching the actor combiner from default to PCGrad on +LN-c+PopArt+FG-c lifts MT50 worst-10 tail tasks from $52.42 \rightarrow 56.50$ (4.08% \uparrow), on top of the 0.83% \uparrow final-mean and worst-10 tail-tasks seed-std stabilization already reported in Section 5.3 and Table 2. We expect the FG-c-only properties of Theorem 1 (combined-gradient norm pinned at \sqrt{K} every minibatch and PopArt absorption via Corollary 1) to matter more in environments with more extreme per-task return-scale heterogeneity than V2 (McLean et al., 2025 App. E.3), even when the headline V2 FG-c vs. PCGrad-c gap is within seed noise; both combiners select different points in the same shared cone $\text{cone}^+\{\mathbf{g}_i^c\}$ (Theorem C.1, Section C.3).

Table D.2: **Per-side combiner asymmetry on MT50 (10 seeds, 100M steps).** Holding $[400 \times 3]$ MLP, PopArt, and LN-c fixed, we vary only the per-side gradient combiner; the asymmetric PCGrad-a + FG-c ($\alpha=1$) row wins, matching the diagnosis that critic gradients suffer scale spread ($497\times$, addressed by scale-invariant FG, Theorem 1) while actor gradients exhibit direction conflict at modest scale spread ($4.1\times$, addressed by PCGrad). FG-c and PCGrad-c are within seed noise (gaps $< \sigma$) and lie in the same shared cone (Theorem C.1); we adopt FG-c for its scale-invariance guarantee.

Actor method	Critic method	MT50 best	MT50 final	MT50 IQM
default	default	90.7 \pm 1.8	88.9 \pm 2.3	89.0
default	FG ($\alpha=1$)	91.2 \pm 2.1	90.0 \pm 2.3	89.7
PCGrad	FG ($\alpha=1$)	92.1 \pm 1.7	90.9 \pm 1.6	90.8
FG ($\alpha=2$)	FG ($\alpha=1$)	90.5 \pm 2.0	89.2 \pm 2.1	89.2
PCGrad	PCGrad	91.9 \pm 1.5	90.5 \pm 1.4	90.4
CAGrad	CAGrad	90.7 \pm 1.3	89.3 \pm 1.4	89.2

D.2 Diagnostic dump-run provenance

The mechanism figures (Figures 2, 3 and D.1 to D.5) are derived from MT10 gradient-snapshot dump runs that are *separate* from the headline 10-seed sweep used for the success-rate tables. Each dump run instruments MultiTaskPPO to write per-task flat actor and critic gradients (plus PopArt σ_i , FairGrad weights when on, long-EMA per-task success rate) to disk every 5 collects (~ 0.5 M env steps, ~ 137 MB per snapshot in fp32) for offline replay. The figures use four such dumps, one per intervention cell:

- **default mean aggregation + PopArt + no LN** — backs the no-LN columns of Figures 3 and D.1.
- **default mean aggregation + PopArt + LN-c** — backs the LN-c columns of Figures 3 and D.1, all of Figures 2 and D.2 (so the $497\times$ vs. $4.1\times$ critic-vs-actor spread is read off the same minibatches), and one column of Figure D.3.
- **FG ($\alpha=2$ actor / $\alpha=1$ critic) + PopArt + no LN** — backs all four panels of Figure D.4 (the FG-trained source keeps every task visibly active on the log-y axis without changing the cols (a, b) per-task ratios) and one column of Figure D.3.
- **FG ($\alpha=2$ actor / $\alpha=1$ critic) + PopArt + LN-c** — backs the per-minibatch realized cell of Figure D.5 (the synthetic scaling-sweep panels of Figure D.5 are generated independently from a Gaussian Gram).

Cols (a, b) of Figure D.4 and the no-PopArt rows of Figure D.1 are obtained by σ^2 -inverting the dumped PopArt-normalized gradient: under PopArt the per-task shared-critic gradient is $\mathbf{g}^{\text{norm}} = \mathbf{g}^{\text{vanilla}}/\sigma_i^2$ because the normalized critic loss is $L_{\text{norm}}^c = (R - V_{\text{raw}})^2/\sigma_i^2$, so multiplying back by σ_i^2 recovers what the unmodified MT-PPO loss would have produced on the same critic-network weights. Figure D.4 cols (c, d) and Figure D.5’s training-time panel additionally rely on offline tight-tolerance FairGrad replay ($\eta = 10^{-13}$ on the y -space Newton solver, vs. production training $\eta = 10^{-2}$); the tight tolerance is needed only for visualization, so that Corollary 1’s (c) \equiv (d) bit-identity is visible at fp64 floor instead of being masked by the $O(10^{-2})$ drift the production solver tolerates.

D.3 Mechanism evidence figures

Critic Gram heatmaps, intervention ablation across stages (Figure D.1).

- PopArt (cols a**→**b, c**→**d) preserves off-diagonal cosines exactly (closed-form identity from per-task σ^{-2} rescaling) and compresses the diagonal magnitude palette in the early/late stages. The MID-row lnC pair shows a transient inversion ($525\times \rightarrow 1428\times$) attributable to the Welford-accumulated σ_i lagging mid-training return-distribution shifts.
- LN (cols a**→**c, b**→**d) reduces off-diagonal direction conflict (early-stage mean off-diag $|\cos|$ from 0.34 no-LN to 0.20 with LN-c on the F3 default-mean dump; the matched FG-trained dump in Figure D.3 reads 0.24 \rightarrow 0.10) while leaving the diagonal magnitude palette roughly intact — a representation-level intervention, not a target-side fix.
- Per-task gradient-norm spread $\max_i \|\mathbf{g}_i^c\| / \min_i \|\mathbf{g}_i^c\|$ (vanilla, σ^2 -inverted) up to $\sim 10,000\times$ at early training, decaying to $\sim 200\times$ by mid-training and rebounding to $\sim 700\times$ by late training under noLN — still orders of magnitude worse than the actor’s 2.7–4.6 \times across the same training stages (Figure D.2).

LN \times FG: algebraically orthogonal critic-Gram health metrics (Figure D.3). Each mechanism targets one health metric and leaves the other un-redressed — LN-c modifies \mathbf{G}^c but does not systematically reduce top-1 weighted contribution mass (which drifts 0.45 \rightarrow 0.57 on this matched-seed pair, within cross-snapshot variability), while FG-c modifies only \mathbf{w} and so cannot affect cosine structure at all. Composing both is required.

FairGrad ($\alpha=1$) equalizes per-task contribution; per-minibatch verification of Corollary 1 (Figure D.4). The (c) \equiv (d) coincidence is the training-time empirical realization of Corollary 1, complementary to the synthetic per-minibatch verification of Theorem 1 in Figure D.5; offline tight-tolerance replay methodology in Section D.2.



Figure D.1: **Critic Gram heatmap matrix: 3 stages (rows: early/mid/late) \times 4 intervention conditions (cols: vanilla, +PopArt, +LN, +PopArt+LN).** Top sidebar = per-task mean-aggregator contribution $\|\mathbf{g}_i\|/K = \sqrt{\mathbf{G}_{ii}}/K$, in-bar badge = per-cell spread $\max_i \|\mathbf{g}_i\| / \min_i \|\mathbf{g}_i\|$; main grid off-diagonal = cosines $\mathbf{G}_{ij}/\sqrt{\mathbf{G}_{ii}\mathbf{G}_{jj}}$; diagonal color = $\log_{10} \mathbf{G}_{ii}$. PopArt (a \rightarrow b, c \rightarrow d) preserves cosines exactly and compresses the diagonal magnitude palette in early/late stages, with a transient mid-row spread inversion under LN-c (525 \times \rightarrow 1428 \times) tracked to Welford-lagged σ_i . LN (a \rightarrow c, b \rightarrow d) reduces off-diagonal conflict at the representation level while leaving the diagonal palette roughly intact.

Theorem 1 verification at fp64 noise floor (Figure D.5). The fp64 L_2 floor of $\sim 10^{-15}$ in panel (b) makes the invariance *bit-identical*, not merely directional — a stronger statement than panel (a)’s $\cos = 1$ alone. Figure D.4 is the training-time analog across MT10 minibatches.

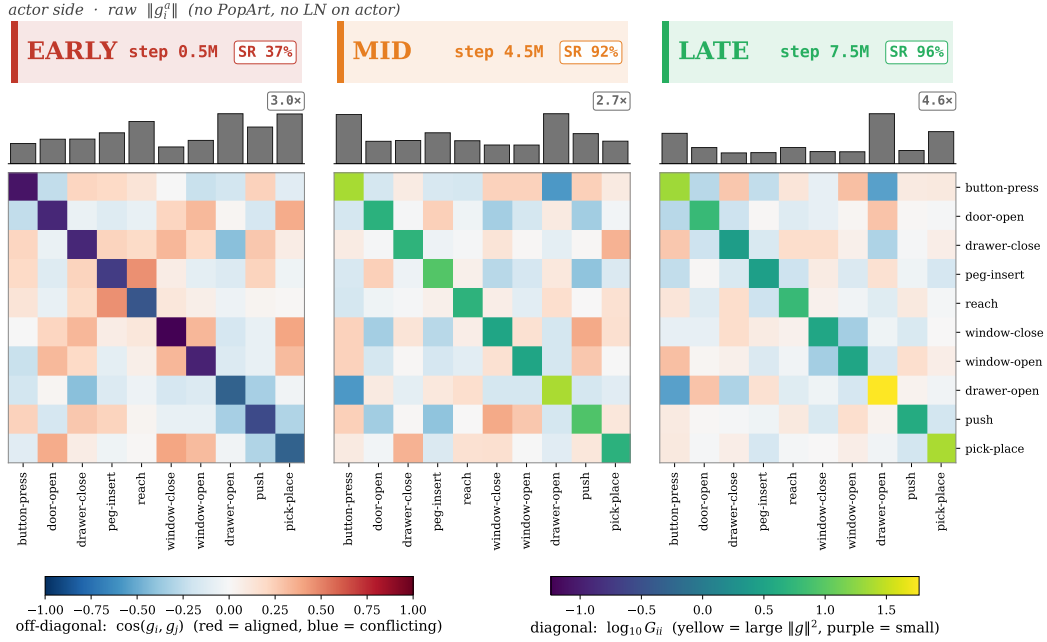


Figure D.2: Actor Gram heatmaps at 3 training stages (EARLY 0.5M / MID 4.5M / LATE 7.5M steps; raw $\|g_i^a\|$, no PopArt or LN on actor). Top sidebar shows per-task gradient-norm bars with the in-bar badge giving the spread ratio $\max_i \|g_i^a\| / \min_i \|g_i^a\|$ ($3.0\times$, $2.7\times$, $4.6\times$); main grid plots off-diagonal cosines $G_{ij} / \sqrt{G_{ii}G_{jj}}$ (red aligned, blue conflicting) with the diagonal colored by $\log_{10} G_{ii}$ (yellow large, purple small). The mild $2.7\text{--}4.6\times$ actor diagonal spread contrasts sharply with the Vanilla MT-PPO critic’s $9864\times$ early spread in Figure D.1, while off-diagonals shift from early inter-task conflict to late near-orthogonal alignment.

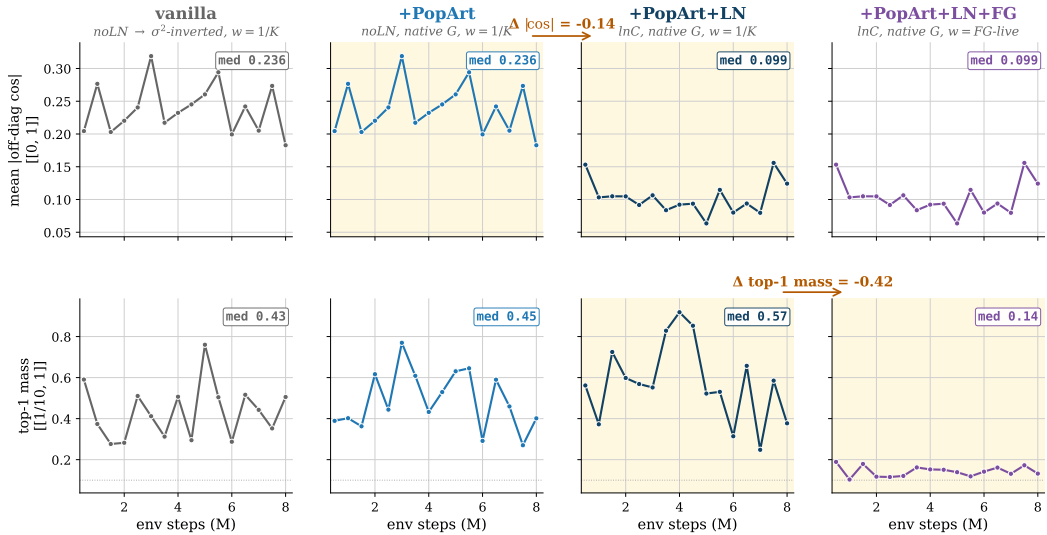


Figure D.3: LN and FG act on algebraically orthogonal critic-Gram health metrics. Top row: mean off-diagonal $|\cos|$; bottom row: top-1 weighted contribution mass. LN (col 2→3) cuts off-diag $|\cos|$ from 0.24 to 0.10 without reducing top-1 mass; FG (col 3→4) cuts top-1 mass to 0.14 while leaving cosine structure unchanged (FG modifies only w , not G).

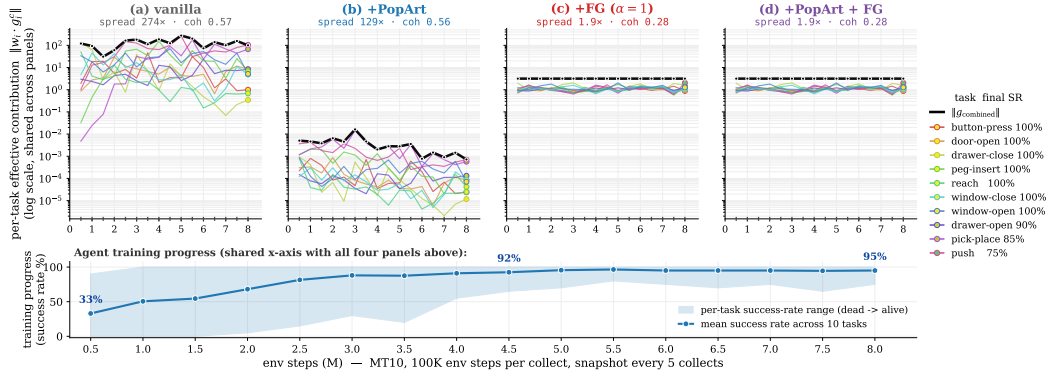


Figure D.4: **FairGrad ($\alpha=1$) equalizes per-task contribution; PopArt’s task-wise rescaling effect is absorbed at the aggregator (Corollary 1).** Per-task effective contribution $\|w_i \mathbf{g}_i^c\|$ across training, with spreads (a) Vanilla MT-PPO $\sim 274\times$, (b) +PopArt $\sim 129\times$, (c) +FG ($\alpha=1$) on raw gradients $\sim 1.9\times$, and (d) +FG ($\alpha=1$) on PopArt-rescaled gradients $\sim 1.9\times$. Panels (c)≡(d) is the per-minibatch corollary of Theorem 1.

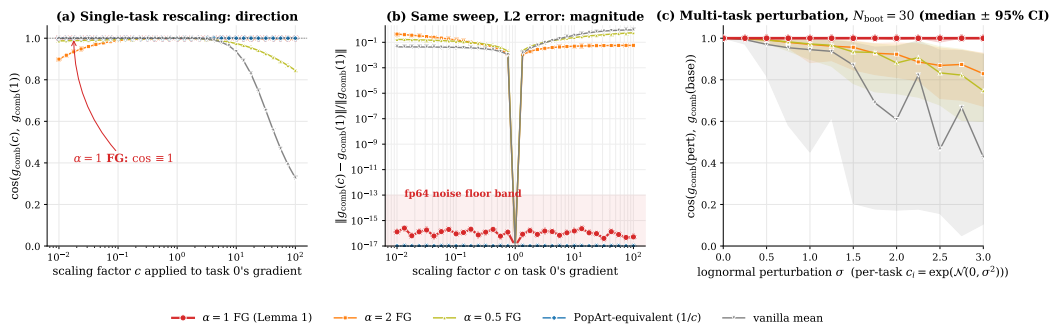


Figure D.5: **Theorem 1 verified at fp64 noise floor.** (a) Single-task scaling sweep over $c \in [10^{-2}, 10^2]$: $\alpha=1$ FG (red) holds $\cos = 1$ exactly while every other combiner dips. (b) Same sweep, L_2 distance: $\alpha=1$ FG sits in the fp64 noise floor ($\sim 10^{-15}$), making the invariance bit-identical rather than merely directional. (c) Multi-task lognormal perturbation $c_i = \exp(\mathcal{N}(0, \sigma^2))$ ($\sigma \in [0, 3]$, $N_{\text{boot}}=30$, median \pm 95% CI): $\alpha=1$ FG stays pinned at $\cos \approx 1$ across the entire range while all other combiners disperse as σ grows.

D.4 Headline V2 learning curves

Figure D.6 provides time-resolved learning curves for the headline numbers in Table 2 and Section 5.2: 10-seed mean \pm std training trajectories on MT10 (panel a, 20M total env steps) and MT50 (panel b, 100M), with each panel’s right-margin endpoint markers reproducing the published ARS-paper V2 baselines at the full-budget endpoint. The MT50 worst- k tail companion is the page-1 teaser Figure 1; the V1 sibling of this figure is Figure D.7 below.

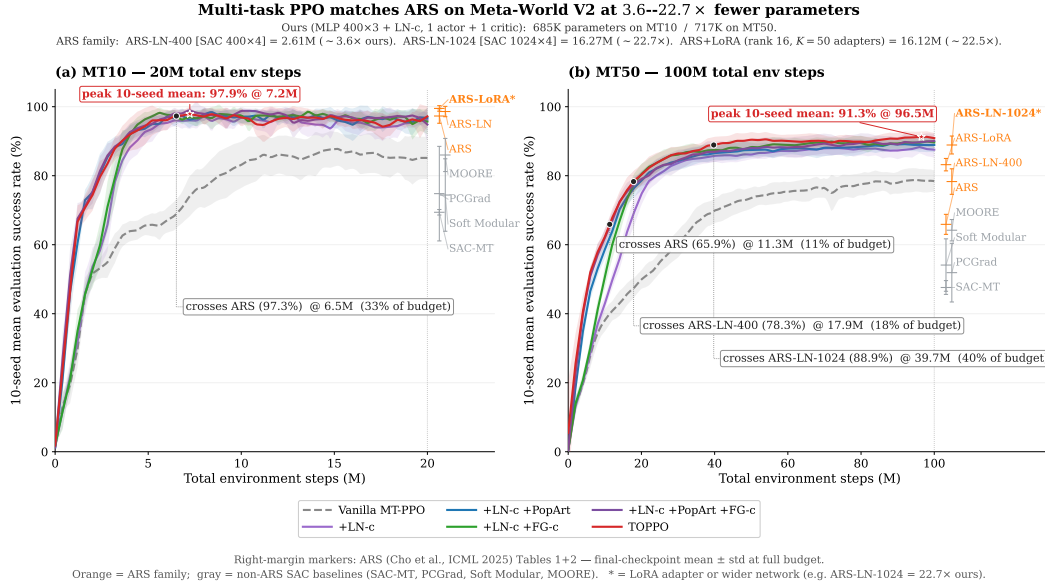


Figure D.6: **MT10 + MT50 V2 learning curves vs. ARS-paper baselines.** 10-seed mean \pm std for the 6 V2 intervention rungs (foreground) on the shared MLP 400×3 backbone (685K params on MT10, 717K on MT50); right-margin markers are full-budget endpoints from Cho et al. [2025] Tables 1–2. (a) MT10 (20M steps): TOPPO peaks at $97.9 \pm 2.1\%$ at 7.2M, matching ARS’s full-budget mean (97.3%) at 33% of budget. (b) MT50 (100M steps): TOPPO peaks at $91.3 \pm 1.6\%$ at 96.5M, crossing every published baseline within $\sim 40\%$ of its own budget (ARS at 11%, ARS-LN-400 at 18%, ARS-LN-1024 at 40%). Asterisks (*) mark methods exceeding our parameter budget (e.g. ARS-LN-1024 = 22.7× ours); the MT50 worst- k tail companion is page-1 teaser Figure 1.

D.5 V1 reward sensitivity

Meta-World V1 rewards have substantially wider per-task scale heterogeneity than V2 [McLean et al., 2025], exactly the regime in which Corollary 1’s scope language predicts PopArt’s non-rescaling channels (Welford running statistics, Adam moments, downstream actor effects through \hat{A}_i) become individually load-bearing. We re-ran the same intervention-stack rungs as Table D.1 plus the PCGrad-a headline on MT50 V1 (10 seeds each, 100M env steps); the upper panel of Table D.3 reports our final-checkpoint mean \pm std alongside the matched V2 number, and the lower panel carries the Meta-World+ MT50 SAC-family V1 baselines [McLean et al., 2025]. The matched-metric V1 head-to-head is in Table 3.

The Corollary 1 signature inversion (PopArt-marginal sign flip across V1/V2) and the V1 head-to-head numbers vs. Meta-World+ baselines are reported in Section 5.3 and Tables 3 and D.3. Two appendix-only mechanism points add to that.

Why FG-c without PopArt hurts on V1. Without PopArt’s value-target normalization, V1’s wide per-task return scales push some tasks’ raw critic gradients into the small-norm regime that the $\alpha=1$ KKT translates into very large w_i ; the post-aggregation $\|\cdot\|_2 \leq 1$ clip then redistributes a fixed budget across an unbalanced set of effective contributions, and the net update lands no better than the unweighted mean. Once PopArt is on (rows 3→5 of Table D.3), FG-c’s V1 IQM marginal recovers to 2.46% \uparrow . PopArt’s value-target normalization is what keeps the per-task gradient norms inside the regime where the $\alpha=1$ KKT solves to a sensible w .

V1→V2 gap: narrower for our PopArt-equipped rows than for the SAC baselines. Under matched final-checkpoint IQM (Table D.3), the headline V1→V2 gap is 11.49% \uparrow ; every fully-stacked row with PopArt on lies in a tight 10% \uparrow to 13% \uparrow band (12.51% \uparrow for +LN-c+PopArt, 10.70% \uparrow for +LN-c+PopArt+FG-c, 11.49% \uparrow for headline). The Meta-World+ SAC-family baselines span 5.19% \uparrow (Soft Modularization) to 40.30% \uparrow (PaCo) under the same V1→V2 reward switch, with three of the five methods showing $\geq 20\%$ \uparrow jumps (MTMHSAC 22.98% \uparrow , PaCo 40.30% \uparrow , PCGrad-SAC 23.65% \uparrow). The narrowness is specifically PopArt’s contribution, not a property of the

Table D.3: **V1-reward sensitivity on MT50**. Intervention rungs of Table D.1 re-run under the original Meta-World V1 rewards (10 seeds, 100M env steps, final-checkpoint IQM \pm std at 25% trim under the Meta-World+ reliable protocol of McLean et al. [2025]); the lower panel transcribes the matched-protocol V1 SAC-family numbers from McLean et al. [2025] Appendix D. V1’s wider per-task return-scale heterogeneity flips the Corollary 1 signature: PopArt’s marginal over LN-c+FG-c grows to 17.01% \uparrow (rows 4 \rightarrow 5) versus 0.32% \uparrow on V2, the regime in which PopArt’s non-rescaling channels become load-bearing rather than absorbed at the FG-c aggregator, and TOPPO clears every V1 SAC baseline by ≥ 17.6 pp under matched-metric IQM (Table 3).

Configuration	V1 IQM	V2 IQM	V1 \rightarrow V2 gap
<i>Our intervention cube (10 seeds, IQM \pm std)</i>			
Vanilla MT-PPO	45.2 \pm 2.4	78.0 \pm 3.3	+32.76
+LN-c	64.3 \pm 3.1	87.7 \pm 2.4	+23.43
+LN-c +PopArt	76.5 \pm 2.0	89.0 \pm 2.3	+12.51
+LN-c +FG-c	62.0 \pm 2.7	89.4 \pm 1.6	+27.39
+LN-c +PopArt +FG-c	79.0 \pm 1.2	89.7 \pm 2.3	+10.70
TOPPO	79.3 \pm 1.3	90.8 \pm 1.6	+11.49
<i>Meta-World+ MT50 SAC-family baselines (10 seeds, IQM \pm std) [McLean et al., 2025]</i>			
MT-MH-SAC	31.9 \pm 2.7	54.9 \pm 1.1	+22.98
Soft Modularization	60.6 \pm 3.9	65.8 \pm 1.9	+5.19
MOORE	61.8 \pm 2.7	72.0 \pm 2.9	+10.22
PaCo	18.6 \pm 15.4	58.9 \pm 4.6	+40.30
PCGrad-SAC	45.8 \pm 5.9	69.5 \pm 2.7	+23.65

Δ_{PopArt} IQM on V1 without FG-c (rows 2 \rightarrow 3): **12.26%** \uparrow . Δ_{PopArt} IQM on V1 with FG-c (rows 4 \rightarrow 5): **17.01%** \uparrow .
On V2 the same two deltas in IQM are 1.35% \uparrow and 0.32% \uparrow respectively.

PPO backbone: our *no*-PopArt rows (vanilla 32.76% \uparrow , +LN-c 23.43% \uparrow , +LN-c+FG-c 27.39% \uparrow) sit in the same 23% \uparrow to 33% \uparrow band as the SAC baselines. Figure D.7 shows the corresponding V1 learning curves on the same axes for each intervention rung.

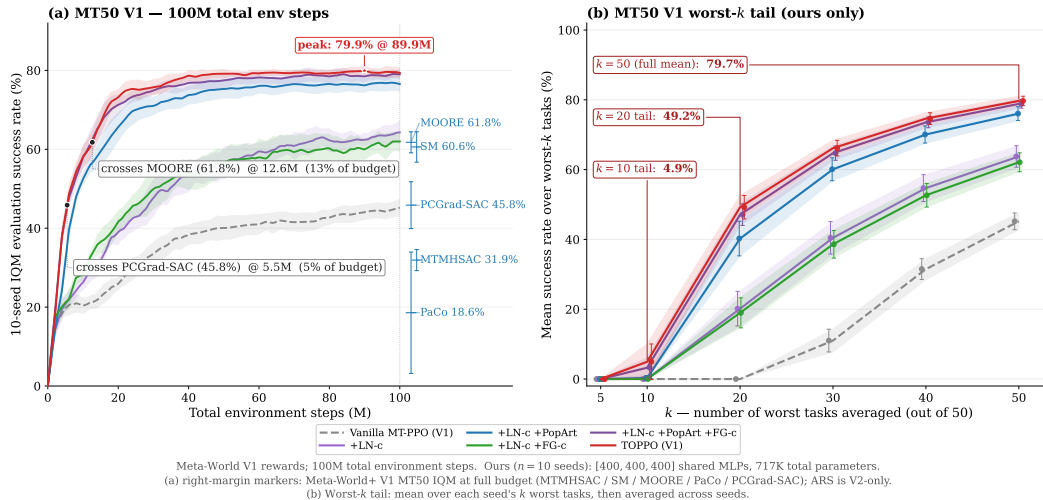


Figure D.7: **MT50 V1 learning curves: intervention stack vs. Meta-World+ V1 baselines**. 10-seed IQM with sample std band on MT50 V1 (100M env steps) for the six intervention rungs of Table D.3, with Meta-World+ V1 IQM baselines [McLean et al., 2025] as right-margin markers (ARS is V2-only). The headline TOPPO V1 stack reaches IQM 79.3% (Table 3), +17.6 pp over MOORE (61.8%). Unlike V2, the V1 ladder makes PopArt the dominant step and FG-c without PopArt tracks LN-c, while the full TOPPO stack remains best.

V1 worst- k tail tasks. The mean/IQM sensitivity above hides how much of V1 remains concentrated in the tail, so Table D.4 reports the same bottom- k diagnostic used for the V2 headline.

Table D.4: **Worst- k tail-tasks success rate on Meta-World MT50 under V1 rewards.** V1 sibling of the V2 worst- k panel in Table 2: per-seed worst- k average for $k \in \{5, 10, 20, 30, 40, 50\}$, then mean \pm std across 10 seeds at the $[400 \times 3]$ MLP backbone, final-checkpoint, across the six intervention-stack rungs from Vanilla MT-PPO to TOPPO. PopArt is the dominant tail step on V1 and FG-c lifts the tail only once PopArt is on; TOPPO is best at every $k \geq 10$. **Bold** = column maximum; $k=5$ is degenerate (0 ± 0 across all rows) and unbolded.

Algorithm	Average Worst- k Success Rate (%)					
	$k=5$	$k=10$	$k=20$	$k=30$	$k=40$	$k=50$
Vanilla MT-PPO	0.0 ± 0.0	0.0 ± 0.0	0.0 ± 0.0	11.0 ± 3.3	31.5 ± 3.0	45.2 ± 2.4
+LN-c	0.0 ± 0.0	0.0 ± 0.1	20.2 ± 5.0	40.5 ± 4.7	54.7 ± 3.8	63.8 ± 3.1
+PopArt +LN-c	0.0 ± 0.0	0.3 ± 0.7	40.2 ± 5.0	60.1 ± 3.3	70.1 ± 2.5	76.1 ± 2.0
+FG-c +LN-c	0.0 ± 0.0	0.0 ± 0.1	19.0 ± 4.3	38.6 ± 4.0	52.6 ± 3.4	62.1 ± 2.7
+PopArt +LN-c +FG-c	0.0 ± 0.0	3.2 ± 2.8	47.1 ± 3.1	64.7 ± 2.1	73.5 ± 1.5	78.8 ± 1.2
PCGrad-a + FG-c + PopArt +LN-c (TOPPO)	0.0 ± 0.0	4.9 ± 5.1	49.2 ± 3.4	66.1 ± 2.2	74.6 ± 1.7	79.7 ± 1.3

Table D.4 is the V1 sibling of Table 2; row-by-row reading is in the table. Three appendix-only points: (i) FG-c without PopArt is worst- k -indistinguishable from LN-c at every k , the worst- k analog of the FG-c-needs-PopArt-on-V1 finding from the mean column. (ii) The dead-task floor on V1 is thicker than V2 (V1 headline $k=10$ is 4.9 ± 5.1 vs. V2 56.5), reflecting that the worst-10 V1 tail tasks have low-density reward shaping that no aggregator can synthesize from a stale critic. (iii) $k=5$ is uniformly 0 ± 0 across all six rows (every V1 seed has ≥ 5 tasks at zero), which is reported as a degenerate column and not bolded.

The V1 per-task table (Table D.7) and per-task learning curves (Figure D.10) are reported alongside the V2 per-task in Section D.6; they expose the FG-c-without-PopArt regression and the thicker V1 dead-task floor row-by-row.

D.6 Per-task success rates

This appendix reports final-checkpoint per-task success (10 seeds, mean \pm std) and the matching per-task learning curves for the three reported regimes: MT10 V2 (Table D.5 and Figure D.8), MT50 V2 (Table D.6 and Figure D.9), and MT50 V1 (Table D.7 and Figure D.10). All tables are sorted worst-first by the TOPPO column; the six columns trace the same cumulative intervention build-up used throughout the paper (Vanilla MT-PPO \rightarrow +LN-c \rightarrow +LN-c+PopArt \rightarrow +LN-c+FG-c \rightarrow +LN-c+PopArt+FG-c \rightarrow TOPPO). Column definitions and bimodal-row ($\sigma > \mu$) reading guidance are in each table caption. The companion learning-curve figures share the same seeds and intervention ladder, so the trajectory leading to each table cell can be read directly — which tasks the Vanilla baseline never lifts off zero, at what step the LN-c rung begins to make hard tasks tractable, and where TOPPO’s PopArt + FG-c + PCGrad-a stack pulls ahead.

MT50 V2 (Table D.6 and Figure D.9). Of the 5 hardest tasks under vanilla MT-PPO (assembly 0.0%, disassemble 0.2%, shelf-place 3.2%, stick-pull 8.6%, pick-place-wall 19.6%), 3/5 recover to $\geq 70\%$ under TOPPO (shelf-place, stick-pull, pick-place-wall); disassemble partially recovers ($0.2 \rightarrow 19.6\%$); only assembly-v3 remains 0% (community-acknowledged unsolvable). TOPPO regresses on push-back ($30.0 \rightarrow 10.0\%$, bimodal $\sigma > \mu$). MT10 V2 saturates near-ceiling under any rung beyond Vanilla MT-PPO (Figure D.8), so the headline-level 4 \rightarrow 6-rung gap is visible only on pick-place-v3 and peg-insert-side-v3; MT10 is reported for completeness while MT50 carries the load-bearing per-task evidence.

MT50 V1 (Table D.7 and Figure D.10). The same drilldown under V1 rewards exposes two regressions diagnosed in Section D.5. (i) *FG-c without PopArt*: the +LN-c+FG-c column tracks +LN-c rather than +LN-c+PopArt on most mid-difficulty tasks (e.g. coffee-pull, lever-pull, handle-pull-side), the per-task realization of the $-2.29\% \downarrow$ V1 IQM regression. (ii) *Thicker dead-task floor*: every rung is pinned at 0% on hand-insert, handle-pull, peg-insert-side, stick-pull, stick-push, accounting for the $k=5$ degenerate column of Table D.4. Where PopArt

does lift LN-c, the gain is concentrated on the same mid-difficulty tasks where TOPPO V1 also pulls ahead, so V1 is the regime in which PopArt’s non-rescaling channels become individually load-bearing rather than absorbed at the FG-c aggregator (Corollary 1).

Table D.5: **Per-task final-checkpoint success on MT10 V2 (10-seed mean \pm std).** Rows are Meta-World MT10 tasks sorted worst-first by TOPPO; the six columns are the cumulative V2 intervention rungs Vanilla MT-PPO \rightarrow +LN-c \rightarrow +LN-c+PopArt \rightarrow +LN-c+FG-c ($\alpha=1$) \rightarrow +LN-c+PopArt+FG-c \rightarrow TOPPO (+PCGrad-a), matching the curves in Figure D.8. Rows with std > mean (e.g. drawer-open-v3 Vanilla, 20.0 ± 42.2) are bimodal across seeds and should be read as a frequency-of-success summary.

Task	Vanilla MT-PPO	+ LN-c	+ LN-c + PopArt	+ LN-c + FG-c	+ LN-c + PopArt + FG-c	TOPPO
pick-place-v3	62.8 \pm 32.8	86.2 \pm 20.0	86.0 \pm 11.7	85.2 \pm 17.2	80.8 \pm 17.3	83.8 \pm 20.9
push-v3	83.2 \pm 27.1	81.6 \pm 28.4	87.6 \pm 19.5	79.8 \pm 25.2	81.8 \pm 24.2	90.8 \pm 14.8
peg-insert-side-v3	98.0 \pm 5.7	97.4 \pm 4.2	99.0 \pm 1.4	94.8 \pm 10.5	85.8 \pm 25.6	98.4 \pm 3.7
button-press-topdown-v3	99.8 \pm 0.6	98.6 \pm 3.3	97.0 \pm 5.9	97.6 \pm 5.4	100.0 \pm 0.0	99.4 \pm 1.3
window-open-v3	98.4 \pm 5.1	99.4 \pm 1.3	99.4 \pm 1.3	99.4 \pm 1.3	100.0 \pm 0.0	99.6 \pm 1.3
door-open-v3	89.6 \pm 31.5	100.0 \pm 0.0	100.0 \pm 0.0	100.0 \pm 0.0	100.0 \pm 0.0	100.0 \pm 0.0
drawer-close-v3	100.0 \pm 0.0	100.0 \pm 0.0	100.0 \pm 0.0	100.0 \pm 0.0	100.0 \pm 0.0	100.0 \pm 0.0
drawer-open-v3	20.0 \pm 42.2	99.0 \pm 3.2	98.6 \pm 4.4	100.0 \pm 0.0	100.0 \pm 0.0	100.0 \pm 0.0
reach-v3	99.8 \pm 0.6	100.0 \pm 0.0	100.0 \pm 0.0	100.0 \pm 0.0	100.0 \pm 0.0	100.0 \pm 0.0
window-close-v3	100.0 \pm 0.0	100.0 \pm 0.0	100.0 \pm 0.0	100.0 \pm 0.0	100.0 \pm 0.0	100.0 \pm 0.0

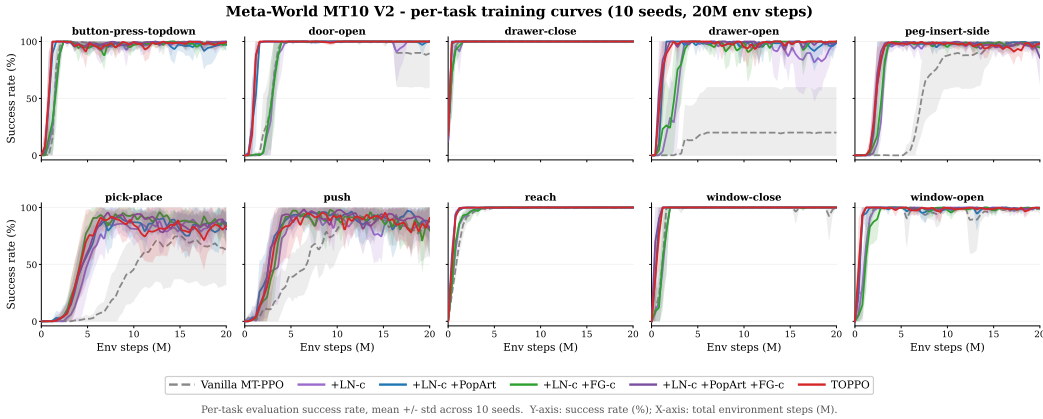


Figure D.8: **Per-task MT10 V2 learning curves (10 seeds, mean \pm std across the 6 V2 intervention rungs).** Companion to Table D.5: ten task panels under the same seeds and 20M-step budget, with Vanilla MT-PPO \rightarrow TOPPO traced as the six curve series. Most tasks saturate near 100% within \sim 5M steps once LN-c is enabled, so the rung-to-rung gap is visible mainly on pick-place-v3 and peg-insert-side-v3, while the load-bearing per-task evidence lives in the MT50 panel below.

Table D.6: **Per-task success rate on MT50 V2 (final-checkpoint, 10-seed mean \pm std).** Tasks sorted ascending by TOPPO mean (worst first). Columns trace the cumulative TOPPO build-up: *Vanilla MT-PPO* (default actor and critic aggregators, no PopArt, no LN), + *LN-c* (add LayerNorm on the critic), + *LN-c + PopArt* (add PopArt return rescaling), + *LN-c + FG-c* (instead add $\alpha=1$ FairGrad on the critic), + *LN-c + PopArt + FG-c* (combine both interventions), and *TOPPO* = + LN-c + PopArt + $\alpha=1$ FG-c + PCGrad-a (full method). Entries with std $>$ mean (e.g. push-back-v3 TOPPO (10.0 \pm 31.6), disassemble-v3 TOPPO (19.6 \pm 40.8)) have a bimodal seed distribution (some seeds at $\sim 0\%$, some near 100%); the reported \pm std should be read as a frequency-of-success summary rather than a Gaussian dispersion in those rows.

Task	Vanilla MT-PPO	+ LN-c	+ LN-c + PopArt	+ LN-c + FG-c	+ LN-c + PopArt + FG-c	TOPPO
assembly-v3	0.0 \pm 0.0	0.0 \pm 0.0	0.2 \pm 0.6	0.0 \pm 0.0	0.0 \pm 0.0	0.0 \pm 0.0
push-back-v3	30.0 \pm 48.3	50.0 \pm 52.7	0.0 \pm 0.0	20.0 \pm 42.2	9.2 \pm 29.1	10.0 \pm 31.6
disassemble-v3	0.2 \pm 0.6	8.0 \pm 25.3	9.4 \pm 29.0	19.0 \pm 40.1	18.6 \pm 39.3	19.6 \pm 40.8
coffee-pull-v3	75.6 \pm 22.8	91.4 \pm 13.0	82.6 \pm 16.3	88.4 \pm 10.3	83.2 \pm 18.6	72.4 \pm 30.6
shelf-place-v3	3.2 \pm 10.1	23.0 \pm 37.9	85.6 \pm 17.4	56.6 \pm 43.8	66.0 \pm 40.2	75.2 \pm 33.4
pick-place-wall-v3	19.6 \pm 41.3	11.2 \pm 31.4	84.8 \pm 30.8	93.4 \pm 10.7	66.6 \pm 46.3	77.2 \pm 40.9
stick-pull-v3	8.6 \pm 27.2	56.4 \pm 39.8	70.4 \pm 29.2	75.8 \pm 28.1	76.2 \pm 23.3	82.4 \pm 11.1
bin-picking-v3	27.4 \pm 43.7	90.0 \pm 8.6	87.8 \pm 8.9	82.4 \pm 29.6	85.0 \pm 16.7	83.4 \pm 29.8
soccer-v3	84.8 \pm 9.6	91.4 \pm 10.3	74.2 \pm 13.0	91.8 \pm 7.8	85.6 \pm 12.6	84.0 \pm 15.0
basketball-v3	34.4 \pm 34.3	72.4 \pm 20.9	75.0 \pm 25.1	76.8 \pm 13.5	80.4 \pm 15.9	85.0 \pm 16.8
coffee-push-v3	83.2 \pm 10.7	95.4 \pm 5.4	94.6 \pm 7.9	84.8 \pm 11.8	92.6 \pm 11.5	90.4 \pm 9.2
button-press-topdown-wall-v3	98.0 \pm 4.3	96.0 \pm 6.0	92.4 \pm 14.0	82.0 \pm 16.1	98.0 \pm 3.5	94.2 \pm 8.9
dial-turn-v3	87.8 \pm 15.1	78.8 \pm 33.9	76.0 \pm 31.2	89.4 \pm 31.4	88.2 \pm 18.7	95.2 \pm 4.4
button-press-topdown-v3	99.0 \pm 2.2	96.4 \pm 6.3	87.6 \pm 15.1	89.8 \pm 9.6	98.0 \pm 3.4	96.4 \pm 5.1
pick-out-of-hole-v3	54.2 \pm 47.6	91.6 \pm 7.0	85.0 \pm 15.2	87.6 \pm 9.5	92.0 \pm 14.0	96.6 \pm 6.4
handle-pull-side-v3	89.8 \pm 31.6	100.0 \pm 0.0	100.0 \pm 0.0	100.0 \pm 0.0	100.0 \pm 0.0	97.4 \pm 8.2
box-close-v3	97.4 \pm 3.0	97.0 \pm 4.2	97.8 \pm 3.9	97.2 \pm 8.2	98.0 \pm 5.0	98.0 \pm 2.9
button-press-wall-v3	99.0 \pm 2.5	96.2 \pm 3.9	98.0 \pm 3.8	99.8 \pm 0.6	98.6 \pm 1.9	98.0 \pm 3.3
hand-insert-v3	98.4 \pm 4.4	94.4 \pm 5.2	99.4 \pm 1.0	99.4 \pm 1.0	97.8 \pm 3.7	98.2 \pm 3.5
push-wall-v3	96.2 \pm 4.6	90.6 \pm 16.2	99.2 \pm 1.4	87.4 \pm 12.4	90.6 \pm 16.1	98.6 \pm 2.1
pick-place-v3	95.2 \pm 5.9	94.8 \pm 5.0	90.8 \pm 15.8	96.0 \pm 5.5	95.2 \pm 8.2	98.8 \pm 1.9
sweep-into-v3	99.0 \pm 2.2	96.6 \pm 5.0	98.4 \pm 1.8	95.8 \pm 6.1	99.4 \pm 1.9	98.8 \pm 3.2
push-v3	90.6 \pm 11.5	90.0 \pm 10.3	95.4 \pm 6.0	92.0 \pm 8.3	97.0 \pm 4.0	99.0 \pm 1.4
hammer-v3	50.0 \pm 52.7	87.8 \pm 31.6	79.8 \pm 42.1	99.8 \pm 0.6	98.2 \pm 5.7	99.2 \pm 1.4
peg-unplug-side-v3	99.0 \pm 1.7	96.0 \pm 8.6	96.2 \pm 9.3	99.6 \pm 0.8	97.0 \pm 3.0	99.2 \pm 1.4
faucet-open-v3	92.8 \pm 16.2	100.0 \pm 0.0	96.0 \pm 8.6	95.6 \pm 7.9	95.8 \pm 13.3	99.4 \pm 1.3
faucet-close-v3	99.2 \pm 1.9	98.8 \pm 2.1	99.6 \pm 0.8	94.6 \pm 11.9	99.6 \pm 0.8	99.6 \pm 1.3
window-open-v3	97.8 \pm 4.7	99.8 \pm 0.6	100.0 \pm 0.0	99.0 \pm 1.9	100.0 \pm 0.0	99.6 \pm 1.3
coffee-button-v3	100.0 \pm 0.0	99.0 \pm 3.2	99.8 \pm 0.6	97.8 \pm 3.8	99.0 \pm 3.2	99.8 \pm 0.6
handle-press-v3	97.8 \pm 4.9	99.8 \pm 0.6	98.2 \pm 2.9	97.6 \pm 6.2	100.0 \pm 0.0	99.8 \pm 0.6
handle-pull-v3	99.8 \pm 0.6	99.8 \pm 0.6	99.8 \pm 0.6	99.6 \pm 0.8	99.8 \pm 0.6	99.8 \pm 0.6
lever-pull-v3	29.2 \pm 47.0	99.4 \pm 1.9	100.0 \pm 0.0	100.0 \pm 0.0	100.0 \pm 0.0	99.8 \pm 0.6
peg-insert-side-v3	99.6 \pm 0.8	99.6 \pm 0.8	100.0 \pm 0.0	99.2 \pm 1.4	98.6 \pm 3.1	99.8 \pm 0.6
reach-wall-v3	98.2 \pm 2.2	99.2 \pm 1.9	99.8 \pm 0.6	98.6 \pm 2.1	99.4 \pm 1.0	99.8 \pm 0.6
sweep-v3	99.8 \pm 0.6	99.4 \pm 1.9	99.6 \pm 0.8	99.4 \pm 1.0	99.2 \pm 1.4	99.8 \pm 0.6
button-press-v3	100.0 \pm 0.0	100.0 \pm 0.0	100.0 \pm 0.0	100.0 \pm 0.0	100.0 \pm 0.0	100.0 \pm 0.0
door-close-v3	100.0 \pm 0.0	100.0 \pm 0.0	100.0 \pm 0.0	100.0 \pm 0.0	100.0 \pm 0.0	100.0 \pm 0.0
door-lock-v3	100.0 \pm 0.0	100.0 \pm 0.0	100.0 \pm 0.0	99.8 \pm 0.6	99.8 \pm 0.6	100.0 \pm 0.0
door-open-v3	99.4 \pm 1.3	100.0 \pm 0.0	100.0 \pm 0.0	100.0 \pm 0.0	100.0 \pm 0.0	100.0 \pm 0.0
door-unlock-v3	100.0 \pm 0.0	100.0 \pm 0.0	100.0 \pm 0.0	100.0 \pm 0.0	100.0 \pm 0.0	100.0 \pm 0.0
drawer-close-v3	100.0 \pm 0.0	100.0 \pm 0.0	100.0 \pm 0.0	100.0 \pm 0.0	100.0 \pm 0.0	100.0 \pm 0.0
drawer-open-v3	30.0 \pm 48.3	89.0 \pm 31.4	97.6 \pm 6.3	97.4 \pm 7.5	100.0 \pm 0.0	100.0 \pm 0.0
handle-press-side-v3	99.2 \pm 1.9	97.8 \pm 4.7	99.4 \pm 1.9	100.0 \pm 0.0	100.0 \pm 0.0	100.0 \pm 0.0
plate-slide-back-side-v3	100.0 \pm 0.0	100.0 \pm 0.0	100.0 \pm 0.0	100.0 \pm 0.0	100.0 \pm 0.0	100.0 \pm 0.0
plate-slide-back-v3	100.0 \pm 0.0	100.0 \pm 0.0	100.0 \pm 0.0	100.0 \pm 0.0	100.0 \pm 0.0	100.0 \pm 0.0
plate-slide-side-v3	100.0 \pm 0.0	100.0 \pm 0.0	100.0 \pm 0.0	100.0 \pm 0.0	100.0 \pm 0.0	100.0 \pm 0.0
plate-slide-v3	100.0 \pm 0.0	100.0 \pm 0.0	100.0 \pm 0.0	100.0 \pm 0.0	100.0 \pm 0.0	100.0 \pm 0.0
reach-v3	99.8 \pm 0.6	100.0 \pm 0.0	100.0 \pm 0.0	100.0 \pm 0.0	100.0 \pm 0.0	100.0 \pm 0.0
stick-push-v3	60.0 \pm 51.2	100.0 \pm 0.0	94.8 \pm 11.0	99.8 \pm 0.6	100.0 \pm 0.0	100.0 \pm 0.0
window-close-v3	99.4 \pm 1.9	100.0 \pm 0.0	100.0 \pm 0.0	100.0 \pm 0.0	100.0 \pm 0.0	100.0 \pm 0.0

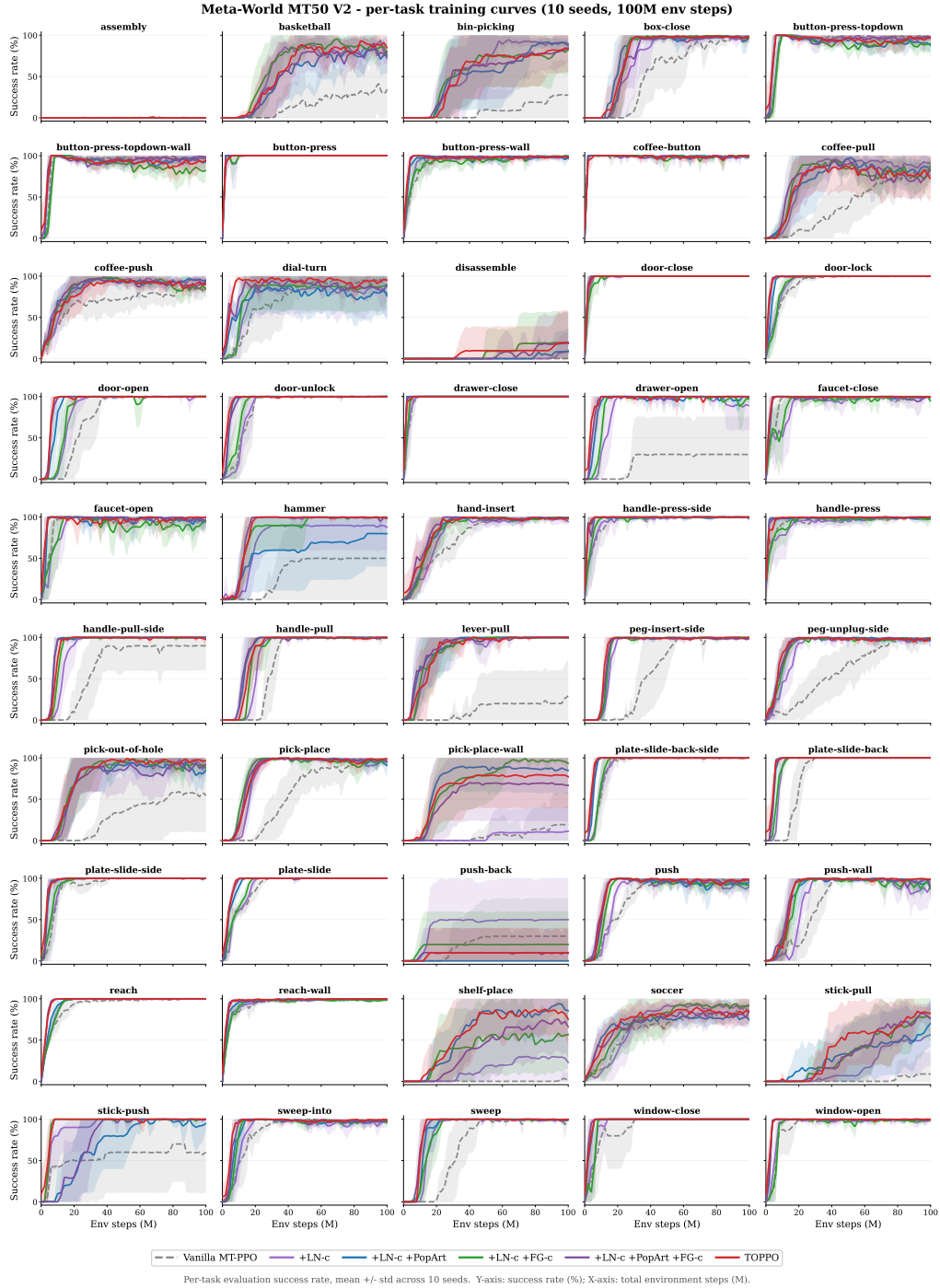


Figure D.9: **Per-task MT50 V2 learning curves: 10-seed mean \pm std for each of the 6 intervention rungs.** Companion to the final-checkpoint MT50 V2 column of Table D.6; same 10 seeds and 100M-step budget. Vanilla MT-PPO (gray) flatlines near 0% on the worst- k tail (assembly, disassemble, shelf-place, stick-pull, pick-place-wall) where LN-c lifts most tasks around 20–40M, PopArt and FG-c add headroom, and TOPPO (red) brings 3/5 of the tail to $\geq 70\%$ by the budget — this figure carries the load-bearing per-task evidence for the headline 4 \rightarrow 6-rung gap.

Table D.7: **Per-task final-checkpoint success on MT50 V1 (10-seed mean \pm std).** Rows are Meta-World MT50 tasks sorted worst-first by TOPPO (V1); the six columns are the cumulative V1 intervention rungs Vanilla MT-PPO \rightarrow +LN-c \rightarrow +LN-c+PopArt \rightarrow +LN-c+FG-c ($\alpha=1$) \rightarrow +LN-c+PopArt+FG-c \rightarrow TOPPO (V1) (+PCGrad-a), matching the curves in Figure D.10; V1’s wider per-task reward scale [McLean et al., 2025] produces a thicker dead-task floor (Table D.4) and the FG-c-without-PopArt regression of Section D.5. Rows with std $>$ mean (e.g. plate-slide-back-v3 Vanilla, 30.0 ± 48.3) are bimodal across seeds and should be read as a frequency-of-success summary.

Task	Vanilla MT-PPO	+ LN-c	+ LN-c + PopArt	+ LN-c + FG-c	+ LN-c + PopArt + FG-c	TOPPO (V1)
box-close-v3	0.0 \pm 0.0	7.4 \pm 11.1	2.2 \pm 7.0	0.4 \pm 1.3	0.0 \pm 0.0	0.0 \pm 0.0
hand-insert-v3	0.0 \pm 0.0	0.0 \pm 0.0	0.0 \pm 0.0	0.0 \pm 0.0	0.0 \pm 0.0	0.0 \pm 0.0
handle-pull-v3	0.0 \pm 0.0	0.0 \pm 0.0	0.0 \pm 0.0	0.0 \pm 0.0	0.0 \pm 0.0	0.0 \pm 0.0
peg-insert-side-v3	0.0 \pm 0.0	0.0 \pm 0.0	0.0 \pm 0.0	0.0 \pm 0.0	0.0 \pm 0.0	0.0 \pm 0.0
stick-pull-v3	0.0 \pm 0.0	0.0 \pm 0.0	0.0 \pm 0.0	0.0 \pm 0.0	0.0 \pm 0.0	0.0 \pm 0.0
stick-push-v3	0.0 \pm 0.0	0.0 \pm 0.0	0.0 \pm 0.0	0.0 \pm 0.0	0.0 \pm 0.0	0.0 \pm 0.0
disassemble-v3	0.0 \pm 0.0	0.0 \pm 0.0	0.0 \pm 0.0	17.8 \pm 37.6	20.0 \pm 42.2	8.6 \pm 27.2
assembly-v3	0.0 \pm 0.0	7.8 \pm 19.4	6.2 \pm 17.5	8.4 \pm 18.3	18.2 \pm 38.5	18.2 \pm 38.1
handle-pull-side-v3	0.0 \pm 0.0	0.0 \pm 0.0	10.0 \pm 31.6	0.0 \pm 0.0	30.0 \pm 48.3	20.0 \pm 42.2
basketball-v3	0.0 \pm 0.0	3.4 \pm 7.5	5.6 \pm 11.7	1.0 \pm 1.9	14.4 \pm 23.5	29.6 \pm 34.2
coffee-pull-v3	18.6 \pm 27.5	40.2 \pm 34.7	7.8 \pm 24.0	30.6 \pm 33.5	40.0 \pm 37.4	68.2 \pm 38.4
hammer-v3	13.0 \pm 24.8	66.4 \pm 36.0	77.2 \pm 23.5	90.2 \pm 14.3	85.4 \pm 12.1	84.2 \pm 13.3
soccer-v3	60.8 \pm 5.4	65.6 \pm 10.1	88.6 \pm 8.0	59.4 \pm 11.7	87.2 \pm 12.6	93.0 \pm 7.0
pick-place-wall-v3	0.0 \pm 0.0	75.4 \pm 21.0	97.6 \pm 3.4	66.0 \pm 29.6	96.8 \pm 3.2	94.8 \pm 4.2
bin-picking-v3	0.0 \pm 0.0	59.8 \pm 17.5	91.8 \pm 7.9	69.2 \pm 18.2	94.2 \pm 6.4	95.4 \pm 5.0
coffee-push-v3	67.4 \pm 9.2	79.2 \pm 12.7	94.6 \pm 4.9	83.4 \pm 6.3	89.8 \pm 11.8	95.6 \pm 5.1
button-press-topdown-v3	100.0 \pm 0.0	91.8 \pm 16.8	99.6 \pm 1.3	84.8 \pm 17.7	98.4 \pm 2.5	95.8 \pm 11.9
button-press-topdown-wall-v3	100.0 \pm 0.0	84.2 \pm 31.2	98.6 \pm 2.7	86.6 \pm 15.0	97.0 \pm 4.6	96.0 \pm 10.0
pick-out-of-hole-v3	0.0 \pm 0.0	69.8 \pm 24.8	72.4 \pm 40.1	70.8 \pm 24.2	97.2 \pm 6.9	96.2 \pm 5.8
push-v3	40.8 \pm 10.1	88.6 \pm 9.0	98.4 \pm 2.6	93.8 \pm 6.0	96.2 \pm 10.1	97.6 \pm 5.6
sweep-into-v3	83.8 \pm 14.1	80.8 \pm 13.1	96.0 \pm 6.2	78.0 \pm 12.2	99.6 \pm 0.8	97.8 \pm 3.8
shelf-place-v3	0.0 \pm 0.0	20.4 \pm 34.8	77.2 \pm 40.9	32.2 \pm 35.5	98.8 \pm 1.7	98.8 \pm 3.3
pick-place-v3	0.0 \pm 0.0	77.8 \pm 14.4	89.2 \pm 31.4	72.2 \pm 15.4	97.6 \pm 2.5	98.6 \pm 2.5
sweep-v3	6.4 \pm 20.2	53.0 \pm 24.0	99.2 \pm 1.4	46.4 \pm 21.1	96.8 \pm 4.6	98.8 \pm 2.7
button-press-wall-v3	71.6 \pm 10.8	81.0 \pm 17.6	98.6 \pm 4.4	67.0 \pm 13.7	98.8 \pm 3.2	99.2 \pm 2.5
door-lock-v3	87.8 \pm 14.3	60.4 \pm 27.6	100.0 \pm 0.0	69.6 \pm 23.7	99.6 \pm 1.3	99.2 \pm 1.7
push-back-v3	0.0 \pm 0.0	76.8 \pm 18.0	97.0 \pm 8.8	54.8 \pm 21.1	99.8 \pm 0.6	99.8 \pm 0.6
push-wall-v3	24.0 \pm 8.1	79.6 \pm 21.4	97.8 \pm 2.7	72.6 \pm 20.1	98.0 \pm 3.8	99.8 \pm 0.6
reach-wall-v3	96.4 \pm 1.8	98.4 \pm 1.8	99.8 \pm 0.6	93.8 \pm 7.3	100.0 \pm 0.0	99.8 \pm 0.6
button-press-v3	100.0 \pm 0.0	100.0 \pm 0.0	100.0 \pm 0.0	94.2 \pm 14.1	99.0 \pm 3.2	100.0 \pm 0.0
coffee-button-v3	100.0 \pm 0.0	100.0 \pm 0.0	100.0 \pm 0.0	100.0 \pm 0.0	100.0 \pm 0.0	100.0 \pm 0.0
dial-turn-v3	84.8 \pm 17.5	95.4 \pm 10.1	99.8 \pm 0.6	86.0 \pm 8.5	100.0 \pm 0.0	100.0 \pm 0.0
door-close-v3	100.0 \pm 0.0	84.0 \pm 22.8	100.0 \pm 0.0	78.4 \pm 20.7	100.0 \pm 0.0	100.0 \pm 0.0
door-open-v3	0.0 \pm 0.0	84.0 \pm 31.2	99.6 \pm 1.3	82.0 \pm 30.5	100.0 \pm 0.0	100.0 \pm 0.0
door-unlock-v3	16.2 \pm 13.9	3.2 \pm 10.1	99.4 \pm 1.0	2.4 \pm 5.1	99.6 \pm 0.8	100.0 \pm 0.0
drawer-close-v3	100.0 \pm 0.0	100.0 \pm 0.0	100.0 \pm 0.0	100.0 \pm 0.0	100.0 \pm 0.0	100.0 \pm 0.0
drawer-open-v3	86.8 \pm 31.7	93.0 \pm 11.6	100.0 \pm 0.0	95.4 \pm 10.1	100.0 \pm 0.0	100.0 \pm 0.0
faucet-close-v3	76.8 \pm 41.0	76.8 \pm 27.1	100.0 \pm 0.0	74.0 \pm 23.9	100.0 \pm 0.0	100.0 \pm 0.0
faucet-open-v3	100.0 \pm 0.0	97.6 \pm 5.0	100.0 \pm 0.0	75.4 \pm 33.1	100.0 \pm 0.0	100.0 \pm 0.0
handle-press-side-v3	100.0 \pm 0.0	100.0 \pm 0.0	100.0 \pm 0.0	99.8 \pm 0.6	100.0 \pm 0.0	100.0 \pm 0.0
handle-press-v3	93.0 \pm 6.2	84.0 \pm 12.1	99.6 \pm 1.3	94.2 \pm 10.5	99.8 \pm 0.6	100.0 \pm 0.0
lever-pull-v3	25.4 \pm 31.2	49.0 \pm 41.3	100.0 \pm 0.0	35.6 \pm 44.6	100.0 \pm 0.0	100.0 \pm 0.0
peg-unplug-side-v3	14.8 \pm 17.3	81.4 \pm 14.5	99.6 \pm 0.8	85.6 \pm 7.5	99.4 \pm 1.9	100.0 \pm 0.0
plate-slide-back-side-v3	18.8 \pm 39.7	100.0 \pm 0.0	100.0 \pm 0.0	99.0 \pm 3.2	100.0 \pm 0.0	100.0 \pm 0.0
plate-slide-back-v3	30.0 \pm 48.3	100.0 \pm 0.0	100.0 \pm 0.0	100.0 \pm 0.0	90.0 \pm 31.6	100.0 \pm 0.0
plate-slide-side-v3	76.4 \pm 40.8	100.0 \pm 0.0	100.0 \pm 0.0	100.0 \pm 0.0	100.0 \pm 0.0	100.0 \pm 0.0
plate-slide-v3	86.2 \pm 13.8	98.2 \pm 4.5	100.0 \pm 0.0	97.0 \pm 5.4	100.0 \pm 0.0	100.0 \pm 0.0
reach-v3	100.0 \pm 0.0	99.8 \pm 0.6	100.0 \pm 0.0	97.6 \pm 3.0	100.0 \pm 0.0	100.0 \pm 0.0
window-close-v3	90.0 \pm 31.6	97.8 \pm 7.0	100.0 \pm 0.0	97.8 \pm 3.2	100.0 \pm 0.0	100.0 \pm 0.0
window-open-v3	90.0 \pm 31.6	76.4 \pm 18.5	99.6 \pm 1.3	62.0 \pm 25.1	100.0 \pm 0.0	100.0 \pm 0.0

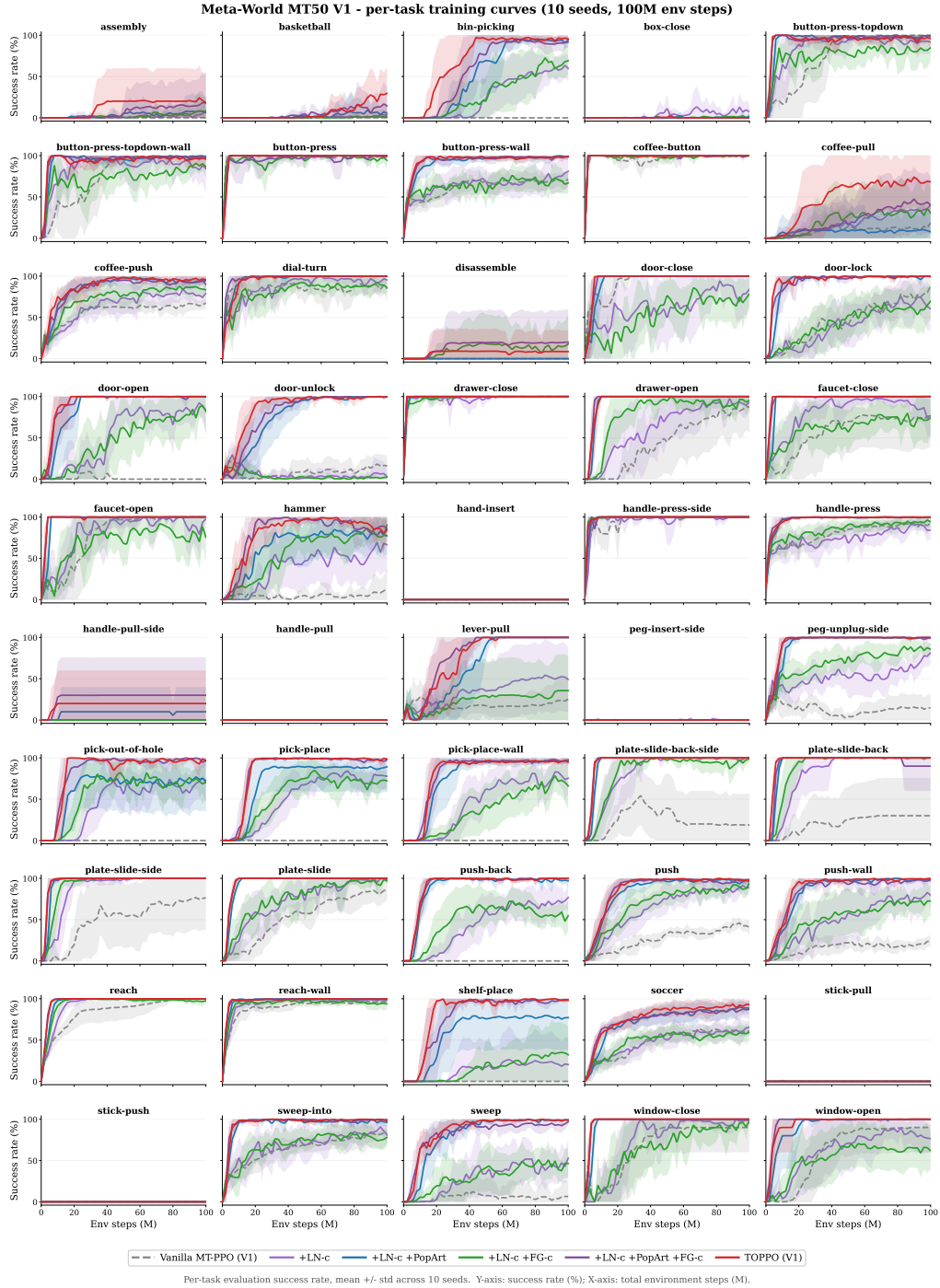


Figure D.10: **Per-task MT50 V1 learning curves: 10-seed mean \pm std for each of the 6 V1 intervention rungs.** Companion to Table D.7; same seeds and 100M-step budget as the V2 panel, run on V1 rewards under the intervention ladder of Table D.3. The V1 dead-task floor is markedly thicker than V2 — several hardest tasks remain at 0% across every rung throughout training (consistent with the $k=5$ degenerate column of Table D.4), the +LN-c+FG-c (no PopArt) trace tracks +LN-c closely on most tasks (the per-task realization of the V1 FG-c-without-PopArt regression in Section D.5), and PopArt’s marginal lift over LN-c concentrates on the same mid-difficulty tasks where TOPPO V1 also pulls ahead (e.g. coffee-pull, lever-pull, handle-pull-side).

D.7 Cross-paper reporting-protocol map

Reporting conventions across the MTRL literature are not standardized: papers differ on the aggregator (final-checkpoint vs. mean-curve peak vs. best-per-seed), the dispersion measure (std vs. SEM vs. IQM), the seed count, and the V1/V2 reward semantics. Table D.9 maps each cited baseline to its source paper’s choices and Table D.8 verifies step-budget alignment; Tables D.10 and D.11 report the four-metric breakdown and per-seed best-checkpoint-step distribution for our headline configurations so readers can convert to any baseline’s protocol. Headline-relevant points beyond what those captions already disclose:

- **SEM vs. std reviewer trap.** The mtrl-codebase family (CAGrad / CARE / FAMO / FairGrad) reports SEM, not std; $SEM \equiv std/\sqrt{n}$ is roughly $3.16\times$ tighter at $n=10$ and is paired with mean-curve-peak aggregation, which is upward-biased. Worked conversions for direct verification: FairGrad MT10 0.84 ± 0.07 SEM $\equiv \pm 0.221$ std; CAGrad MT10 0.83 ± 0.045 SEM $\equiv \pm 0.142$ std; CAGrad MT50 0.52 ± 0.023 SEM $\equiv \pm 0.073$ std.
- **Step-budget alignment is exact.** All cited baselines except Soft Modularization (15M/50M paper-original; we cite the MW+ 20M/100M re-run instead) train at our 20M/100M budget, so direct comparison is valid without renormalization. The unannotated Meta-World+ MT50 numbers are validated against the companion `metaworld-algorithms` repo configs (including the misnamed `paco_mt10.py` file whose internal config is verbatim MT50 K=20); details in Table D.8 caption.
- **V1→V2 disadvantage acknowledgment.** CAGrad / CARE / FAMO / FairGrad were pinned to a pre-V2 Meta-World commit and report V1 numbers; Meta-World+ App. E.3 documents that all tested algorithms perform better on V2 than V1, so the V1-baseline / V2-ours comparison in Table 2 is mildly unfavorable to us in absolute level. The V1/V2 sensitivity sweep in Section D.5 reports both rewards on the same TOPPO stack so the cross-version effect can be read directly.

Table D.8: **Step-budget alignment across cited baselines.** We normalize every paper’s reporting convention — “per-task”, “per mtrl-iteration”, “epochs \times batch” — to total environment steps (every parallel-env step counts +1) and verify all rows train at our 20M/100M budget except Soft Modularization (15M/50M paper-original; we cite its Meta-World+ re-run instead), so cross-paper comparison in Table 2 requires no renormalization.

Paper	Reported	Total MT10	Total MT50	Verification
Ours (PPO)	20M / 100M (total)	20M	100M	baseline
Original Meta-World (2020)	500 epochs \times batch	20M	100M	verified from garage scripts
CAGrad (2021)	2M (mtrl iter)	20M	100M	<code>num_envs = num_tasks</code>
CARE (2021)	2M per task	20M	100M	explicit
FAMO (2023)	follows CAGrad exactly	20M	–	MT10 only
FairGrad (2024)	2M / batch 1280	20M	–	MT10 only
PaCo (2022)	20M total / 100M total	20M	100M	explicit
MOORE (2024)	20 ep \times 100K vec \times envs	20M	100M	verified from <code>VecCore</code>
ARS (2025)	$2 \cdot 10^7 / 10^8$	20M	100M	matches ours exactly
Soft Modularization (2020)	15M / 50M	15M	50M	outlier; verified from JSON configs
Meta-World+ (2025) multi-task	not explicitly tabulated	20M	100M	inferred from companion repo (Section D.7)

Table D.9: **Reporting protocol across cited baselines.** For each cited paper we tabulate seed count, aggregator (A: final-checkpoint average; B: best-per-seed then average; C: mean-curve peak; D: late-window mean; E: other), dispersion measure (std / SEM / IQM), eval episodes per task, and reward version, so readers can align cross-paper comparisons in Tables 2 to 3 with the matching column of Table D.10. V1* marks rows inferred from a pinned pre-V2 Meta-World commit; † Meta-World+ Appendix D scalar tables carry no explicit dispersion label, the paper’s main text only commits to 95% CIs for the IQM-through-training plots, and the companion `metaworld-algorithms` repository contains no table-generation / cross-seed aggregation script – so whether the reported \pm is std, SEM, or a 95% CI cannot be verified from primary sources. We treat it as std throughout the paper (Tables 3 and D.3, the V1 head-to-head); this is a working assumption.

Paper	Seeds	Aggreg.	Description	Disp.	Eval eps.	Reward
Ours (PPO)	10	all of A/B/C/D	best/peak/final/late, all reported	std	50	V2
MT-SAC (orig 2020)	10	(E)	max-over-time per (seed,task)	none	5	V1
Soft-Mod (2020)	3	(E)	final-policy 100-ep dedicated pass	(graphical only)	100	V1
PCGrad (2020)	?	–	figure eyeball, no num table	–	?	V1
CAGrad (2021)	10	(C)	mean-curve peak (App B.3)	SEM	1	V1*
CARE (2021)	10	(C)	mean-curve peak	SEM	5	V1
PaCo (2022)	10	(A)	final 20M, explicit anti-peak	std	10	V2
FAMO (2023)	10	(C)	inherits CAGrad	SEM	1	V1*
MOORE (2024)	10	(A)	final ckpt (20M MT10 / 100M MT50)	std	10	V2
FairGrad (2024)	10	(C)	mean-curve peak (§5.3)	SEM	1	V1*
Meta-World+ (2025)	10	(A/B) [?]	IQM (final-step or best ckpt; ambiguous)	IQM, \pm unspec. [†]	50	V1+V2
ARS (2025)	8	(A)	final EvalFinalSR	std	10	V2

Table D.10: **Four-metric disclosure for our headline configurations.** Each row reports MT10 and MT50 success (% , mean \pm std over 10 seeds at 20M / 100M total environment steps) under four aggregators that span the conventions used by cited baselines: *best* (per-seed argmax then averaged), *peak* (argmax of the mean curve), *final* (terminal step), and *late* (mean of the last 10% of steps). Reporting all four lets readers convert our numbers to any baseline’s protocol (Table D.9).

Configuration	MT10				MT50			
	best	peak	final	late	best	peak	final	late
Vanilla MT-PPO	89.5 \pm 4.6	87.8 \pm 5.1	85.2 \pm 6.5	85.1 \pm 5.7	79.6 \pm 3.2	78.7 \pm 3.7	78.5 \pm 3.3	78.5 \pm 3.5
+LN-c	99.5 \pm 0.3	97.9 \pm 1.6	96.2 \pm 3.4	95.3 \pm 1.9	89.2 \pm 1.9	88.3 \pm 1.9	87.5 \pm 2.4	87.7 \pm 2.2
+LN-c +PopArt	99.9 \pm 0.2	98.5 \pm 1.2	96.8 \pm 1.5	96.4 \pm 2.3	90.7 \pm 1.8	89.2 \pm 2.2	88.9 \pm 2.3	89.0 \pm 1.8
+LN-c +FG-c	99.8 \pm 0.2	98.6 \pm 0.7	95.7 \pm 4.0	96.2 \pm 2.4	91.2 \pm 1.6	89.9 \pm 1.7	89.7 \pm 1.6	89.6 \pm 1.5
+LN-c +PopArt +FG-c	99.8 \pm 0.2	99.0 \pm 0.6	94.8 \pm 5.1	96.7 \pm 2.0	91.2 \pm 2.1	90.1 \pm 2.3	90.1 \pm 2.3	89.7 \pm 2.2
+PCGrad-a (TOPPO)	99.6 \pm 0.4	97.9 \pm 2.2	97.2 \pm 3.1	96.0 \pm 1.6	92.1 \pm 1.7	91.3 \pm 1.6	90.9 \pm 1.6	91.0 \pm 1.7

Table D.11: **Per-seed best-checkpoint step distribution** (median, IQR, min–max in env-step millions across 10 seeds, per configuration). Best-per-seed is the protocol used by the mtrl-codebase baselines in Table D.9; medians well before the 20M/100M endpoint show that end-of-budget reporting would systematically understate these stacks, so apples-to-apples comparison requires the per-seed peak rather than the final checkpoint.

Configuration	Bench.	Budget (M)	Median (M)	IQR (M)	min–max (M)
Vanilla MT-PPO	MT10	20	15.0	[13.4, 17.2]	10.0–19.6
+LN-c	MT10	20	11.8	[10.9, 16.4]	6.8–20.0
+LN-c +PopArt	MT10	20	13.4	[9.7, 15.9]	6.4–17.6
+LN-c +FG-c	MT10	20	8.4	[6.7, 9.7]	5.6–19.2
+LN-c +PopArt +FG-c	MT10	20	8.4	[7.0, 9.8]	6.4–12.4
+PCGrad-a (TOPPO)	MT10	20	12.6	[9.4, 17.2]	7.2–19.6
Vanilla MT-PPO	MT50	100	93.5	[89.0, 97.2]	83.0–99.0
+LN-c	MT50	100	77.0	[72.0, 86.5]	48.0–96.0
+LN-c +PopArt	MT50	100	88.0	[67.0, 92.0]	40.0–96.0
+LN-c +FG-c	MT50	100	84.0	[70.0, 97.0]	58.0–100.0
+LN-c +PopArt +FG-c	MT50	100	86.0	[66.0, 97.5]	40.0–100.0
+PCGrad-a (TOPPO)	MT50	100	84.0	[51.0, 93.5]	46.0–96.0